A Performance Study of Reluctance Synchronous Machines Fed by Non Sinusoidal Currents

Michiel Hendrik Albertus Prins

A Performance Study of Reluctance Synchronous Machines Fed by Non Sinusoidal Currents

By

MICHIEL HENDRIK ALBERTUS PRINS

Submitted to the Department of Electrical Engineering in Fulfilment of the Requirements for the Magister Technologiae in Electrical Engineering at the
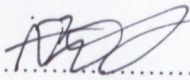
Cape Peninsula University of Technology

SUPERVISOR: E. VOSS

December 2011

Declaration

I, MICHIEL HENDRIK ALBERTUS PRINS, submit this thesis in fulfilment of the requirements for the degree of Magister Technologiae (MTech) in Electrical Engineering.

I claim that this is my own original work and that it has not been submitted in this or similar form for a degree at any other tertiary institution.

....

Albertu Prins
Candidate

.... 26/03/12 ....

Date

ii

Acknowledgements

I wish to express my gratitude to all of the following:

Synopsis

Reluctance synchronous Machines (RSM's) have become a viable alternative for alternating current (ac) drives since electronic drives have improved. These electronic drives make use of static switching devices to control the speed and torque of ac machines. The output waveforms of these devices contain numerous harmonics which can have harmful effects on some of the machine's performance parameters. Performance parameters of the RSM include torque, torque ripple, power, power factor and efficiency which are essential for the machine designer as well as the user. Poor efficiency of the RSM is mainly due to the copper losses of the stator windings and core losses in the stator iron. The core losses primarily consist of hysteresis- and eddy-current losses as well as additional losses which are due to domain wall rotation and pinning. Unlike the Induction Machine (IM), the RSM has no copper losses in the rotor, which reduces the operating temperature of the machine considerably.

This thesis will focus on the influence non sinusoidal currents have on the performance parameters of a RSM. The machine will be subjected to ideal harmonics created by a six pulse drive which are theoretically predicted based on the operation of a six pulse drive. The machine will also be subjected to published data which are measured data for a more practical approach. These two cases will be compared to rated operating conditions.

Table of Content

List of Figures and Tables

List of Symbols and Abbreviations

Roman Alphabet

$\bar{A}$	magnetic vector potential (Vs/m)
A_{avgGO}	average magnetic vector potential at the enter side of a coil (Vs/m)
A_{avgRE}	average magnetic vector potential at the return side of a coil (Vs/m)
$A_{(GOB1,2,3)}$	average magnetic vector potential at enter side of phase B (Vs/m)
$A_{(GOR1,2,3)}$	average magnetic vector potential at enter side of phase R (Vs/m)
$A_{(GOY1,2,3)}$	average magnetic vector potential at enter side of phase Y (Vs/m)
$A_{(REB1,2,3)}$	average magnetic vector potential at return side of phase B (Vs/m)
$A_{(RER1,2,3)}$	average magnetic vector potential at return side of phase R (Vs/m)
$A_{(REY1,2,3)}$	average magnetic vector potential at return side of phase Y (Vs/m)
A_z	vector potential component in z-axis direction (Vs/m)
$\bar{B}$	flux density (Vs/m^2)
B_n	normal vector component of flux density (Vs/m^2)
B_t	tangential vector component of flux density (Vs/m^2)
$\bar{F}$	electromagnetic force (N)
I_n	input rms supply current of the nth harmonic order (A)
I_{ph}	phase rms current (A)
$\bar{I}_S$	current space phasor (A $\angle$ deg)
i_B	instantaneous current in phase B (A)
i_{dqo}	instantaneous values of the d, q and 0 component currents (A)
i_R	instantaneous current in phase R (A)
i_{RYB}	instantaneous values of the R, Y and B phase currents (A)
i_Y	instantaneous current in phase Y (A)
i_d	steady state d-axis stator current (A)

i_q	steady state q-axis stator current (A)
i_0	zero sequence component of the stator current (A)
$[K]$	Park's transformation matrix
L_d	d-axis synchronous inductance (Vs/A)
L_q	q-axis synchronous inductance (Vs/A)
ℓ	effective winding length in the z direction (m)
ℓ_s	effective rotor stack length (m)
N	number of turns per coil
N_{ph}	number of turns per phase
P_{cu}	copper loss (W)
P_f	power factor
P_{out}	developed output power (W)
r	radius to the centre of the air-gap (m)
r_s	resistance of all the conductors of a phase winding (Ω)
$\bar{S}$	area of integration (m^2)
T	electromagnetic torque (Nm)
T_{avg}	average torque (Nm)
T_{max}	maximum instantaneous torque (Nm)
T_{min}	minimum instantaneous torque (Nm)
T_{ripple}	torque ripple (%)

Greek Alphabet

Γ	contour of integration (m)
γ	torque angle (deg)
δ	angle of stator flux linkage space phasor (deg)
η	efficiency (%)
ϕ	angle of current space phasor referenced to rotor d-axis (deg)
λ	flux linkage of a given coil (Vs)
λ_R	instantaneous flux linkage in phase R (Vs)

λ_B	instantaneous flux linkage in phase B (Vs)
λ_Y	instantaneous flux linkage in phase Y (Vs)
λ_d	d-axis fundamental stator flux linkage component (Vs)
λ_q	q-axis fundamental stator flux linkage component (Vs)
λ_0	zero sequence component of the stator flux linkage component (Vs)
λ_S	flux linkage space phasor (Vs $\angle$ deg)
μ_0	permeability of free space (Vs/Am)
σ	saliency ratio of L_d / L_q
σ_n	normal stress vector component (N/m)
$\bar{\sigma}_s$	resultant surface stress (N/m)
σ_t	tangential stress vector component (N/m)
υ	qd-current ratio, i_q / i_d
ω	reference frame rotating speed (deg/s)

Abbreviations:

FE	Finite Element
IM	Induction Machine
MST	Maxwell Stress Tensor
RSM	Reluctance Synchronous Machine
SRM	Switched Reluctance Machine

1. Introduction

1.1   The development of RSM's

The phenomena of synchronous reluctance machines was observed by Siemens, a German engineer, who found that the excitation of a single phase motor can be suppressed without stopping it as early as 1874 (Blondel, 1913). In the early 1900s research was done by Thompson (1902) on a salient-type rotor, a rotor having different reluctance paths in the d- and q-axis, with a slitted field pole where he found that armature reaction was reduced. Quadrature reaction was reduced but not sufficiently. The latter however made an important contribution to anisotropic field structures. Approximately 20 years later Kostko (1923) investigated a more cylindrical rotor shape with flux barriers.

Between the mid 1940s and early 1950s calculations on performance parameters were done by Tricky (1946), Talaat (1951) and Lin (1951). Lin used equivalent circuits to simplify and improve the analysis of reluctance machines.

In 1956 the main concern was rotor geometries used to increase reluctance torque (Douglas, 1956). He proposed a slitted rotor core to find a permeance ratio. The idea of the slitted rotor core arose from the research of Thompson (1902). It was found that slitting didn't have a big effect on the performance of salient-pole machines. Finite Element (FE) software was unavailable up to this phase and all models were theory-based.

Between the late 1960s and the early 1970s attention was directed towards stability problems. Research was conducted by Lipo & Krause (1967) and in the same year by Lawrenson & Gupta (1967) who investigated rotor cut-outs and the effect when the cut-outs are filled with conducting material. Cruickskank et al. (1971) were the first to investigate the possibilities of axially laminated rotors. This created a study by Lipo & Matsuo (1994) on the optimization of axially laminated rotors. They looked at the ratio of the rotor insulation width to the rotor iron width to obtain maximum torque production. Results showed that a ratio of 0.2 to 0.6 showed good torque production. From the 1970s onwards attention was drawn to single-salient RSM rotors. Honsinger (1971) analyzed a two flux barrier per pole rotor where he developed equations for L_d and L_q. Later the d- and q-inductances and the affect of cross-magnetisation were investigated by Kamper & Volschenk (1994) on a two flux barrier per pole RSM. Kamper states that the machine can either be designed for a high power factor or a high torque rating, or for an optimum between these two since a high induction ratio is

needed for high power factor, alternatively a high induction difference for a high torque rating.

From the 1990s until present torque ripple reduction of RSMs, this is in fact stabilizing the machine, created more interest than before. Fratta et al. (1993) investigated a multiple segment rotor and the effect stator teeth have on the torque ripple. They state that the most straightforward way to compensate for one harmonic component of torque ripple is to divide the rotor in two sections, shifted with respect to each other. They managed to reduce torque ripple but a complete compensation was not achievable due to the rotor's anisotropy. This statement was verified by Vagati et al. (1998).

Later Kamper & Bomela (2002) investigated the effect of rotor skewing and stator chording on the torque, power factor and torque ripple. Results were confirmed by FE analysis using the time-stepping method. They found that chording reduces average torque and power rating significantly with little effect on torque ripple. On the other hand skewing has little effect on average torque and power factor when skewed by one stator slot while a large drop in the two quantities occurs when skewed by two stator slots and the torque ripple is reduced significantly. In that same year Kamper & Fick (2002) investigated constant current angle control which enables them to run the RSM at near optimum efficiency.

Two years later Sanada et al. (2004) looked at asymmetrical flux barrier arrangements to improve torque ripple. He found that the torque ripple decreased without a decrease in average torque but the dynamic balance of the rotor collapsed and caused vibration, which was a setback.

Bianchi et al. (2009) investigated different rotor flux barrier geometries to reduce the torque ripple. They looked at rotors with two flux barriers per pole, different flux barriers per pole and flux barriers with inserted permanent magnets to saturate the iron bridges.

Lee et al. (2004) investigated switched reluctance synchronous machines. A new design arose which incorporated a rotor having notched teeth which reduced the torque ripple by 3.5% - 5%. The average torque decreased by 0.8%.

Hoffmann & Sanders (2000) focussed on a design to minimize rotor losses thereby increasing the efficiency. They investigated a solid rotor design for high speed application with bonded sections of ferromagnetic and nonmagnetic steel. Stator design was also investigated to minimize winding and slot harmonics which generate rotor losses.

All of the above-mentioned authors based their research on different rotor geometries but concentrated mainly on ways to reduce torque ripple and increase average torque.

No attention was directed towards the performance parameters (Torque, Torque ripple, Power, Power Factor and Efficiency) when the input currents to the RSM are non sinusoidal. There are a number of authors who investigated induction machines when fed by non sinusoidal currents. Important publications are those of Eguiluz (1999) who investigated additional losses caused to induction motors when the supply consist of harmonics and Singh (2005) who looked into the effects harmonics have which are fed by electronic drives.

The aim of this thesis is to perform a clearly outlined analysis on the effects non sinusoidal input currents have on the performance parameters of the RSM.

1.2   Problem statement

Electronic drives are widely used today as they have plenty of benefits. One of these benefits is that a large direct and quadrature inductance difference and ratio can be achieved. This results in a higher average torque and increased average power factor. It is most desirable for electrical machines to operate from clean sinusoidal waveforms but unfortunately the output of electronic drives is distorted which can have undesirable effects on the performance of the machines. These distorted waveforms contain numerous current harmonics whose magnitudes are theoretically predicted to be the fundamental current divided by the harmonic order shown in equation (1.2.1), and are called in this thesis *ideal harmonic* data.

$$I_n = \frac{I_1}{n} \qquad\qquad (1.2.1)$$

where I_n is the current magnitude of the nth harmonic order and I_1 the magnitude of the fundamental current.

Practical measurements show that these predictions are not entirely accurate. This is verified by Anonymous (2000). The practical measurements, done by companies selling six pulse drives, are tabulated and given as a percentage of the fundamental current magnitude for each harmonic order. This tabulated data are called in this thesis *published harmonic* data.

To the knowledge of the author no attention has been directed towards the performance parameters of RSM's when subjected to non sinusoidal input currents.

The first problem statement is therefore: "How will ideal harmonic currents created by electronic drives influence the performance parameters of a RSM?"

And the second problem statement is: "How will published harmonic currents created by electronic drives influence the performance parameters of a RSM.

4

1.3   Problem approach

Contributions have been made towards improved performance of RSM's by numerous researchers while RSM's subjected to non sinusoidal input currents have not been researched since the beginning according to the author's knowledge. This provided the opportunity to investigate the situation where the machine is subjected to non sinusoidal currents created by a six-pulse drive. The machine that will be used is a four pole 5.5kW single salient vector controlled RSM. The stator structure consists of a 36 slot full pitched single layer winding with open slots. The rotor structure used will be that of Hanekom (2006) whose rotor has a single barrier structure with a barrier pitch of 26° mech. and no cut-outs (Appendix B) as shown in Fig 1.3.1.
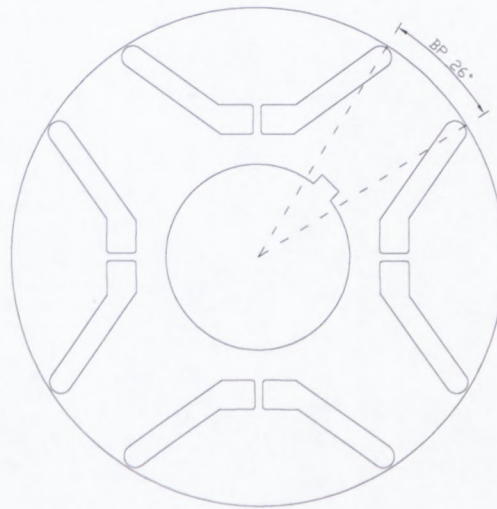
Fig. 1.3.1 Cross sectional view of the rotor of the 5.5kW RSM

The aim of this work is to obtain the performance parameters of the machine under ideal and published harmonic current conditions and compare the results to each other and to fundamental current conditions. The first part of this thesis will focus on the basic quantities of the RSM and how they are calculated. The machine will be modelled using a FE software along a path through the centre of the air-gap. Results will be obtained as the rotor move through one pole pitch in steps of one degree electrical. At first the machine will be modelled with rated sinusoidal input currents and performance properties will be calculated and analyzed. The parameters investigated are the following: Torque, Torque ripple, Power, Power factor and Efficiency. From there the approach is to add ideal current harmonics of a

six-pulse drive to the fundamental current and obtain the performance parameters. The performance of the ideal current harmonics of the six-pulse drive will then be compared to the performance obtained from rated sinusoidal input currents. Winding losses will be investigated as they influence the overall performance of the RSM. After simulating the ideal current harmonics the published current harmonics of the six pulse drive will be simulated for a more practical approach as the ideal harmonics are theoretically predicted. Performance properties of the published harmonic data will be examined similar to the ideal harmonics and will be compared to the rated performance and to the performance when ideal current harmonics are added to the fundamental currents. For both cases individual current harmonics will be removed to see the effect of each current harmonic on the performance parameters.

1.4   Outline of thesis

The layout of the remaining part of the thesis is as follows.

Chapter 2:   In this chapter the calculation of performance parameters will be shown from fundamental quantities.

Chapter 3:   In this section the performance parameters of the RSM will be calculated under rated/fundamental current conditions. These results will be used to compare the performance of the machine to the performance when fed with non sinusoidal currents. In closing a summary of the findings will be given.

Chapter 4:   In this section the machine will be subjected to ideal current harmonics from a six-pulse drive. The effect on the performance parameters will be investigated and electrical losses will be calculated. The effect of individual current harmonics is also investigated. Results will be compared to rated operating conditions and a summary of the findings will be given.

Chapter 5:   In this chapter the RSM will be subjected to published current harmonics of a six-pulse drive to give a more practical representation. Like in chapter 4 the performance parameters will be investigated and losses will be calculated. The effect of individual current harmonics is also investigated. The results will be compared to rated operating conditions and to ideal current harmonic conditions. In closing a summary of the findings will be given.

Chapter 6:   This chapter will conclude on how non sinusoidal input currents influence the performance parameters of the RSM. Recommendations will be given and areas not covered in this work will be indicated for future research.

2. Overview of a RSM

This section describes the torque-, torque ripple-, power factor-, output power- and efficiency as a function of the rotor position of the RSM. With the presence of electronic drives used for control the opportunity presents itself to investigate the effect non-sinusoidal input currents have on performance parameters. This will be discussed in the following chapters. The performance parameters will be derived from fundamental variables for rated conditions. This work will only deal with steady state machine operation and therefore the calculations and derivations will be based on the latter. The input current harmonics supplied to the RSM in this thesis are time dependant.

2.1 Performance parameters

2.1.1 Calculation of torque and torque ripple

The torque of the RSM is calculated in the FE program using Maxwell's Stress Tensor (MST) method who created a set of equations which explained the magnetic field phenomena by a longitudinal tension and a transverse pressure both equal in magnitude (Howe, 1935). Maxwell proposed that the total electromagnetic force on a body can be calculated by integrating the stresses over an arbitrary surface enclosing the body (Wignall et el., 1988), shown in equation (2.1.1). The FE solution is time varying as the rotor moves through one pole pitch. Since the FE solution are using the time stepping method the fields can be considered as static for each rotor position and the electromagnetic force over the surface are calculated by

$$\bar{F} = \oint_S \bar{\sigma}_s \cdot d\bar{S} \tag{2.1.1}$$

where $\bar{F}$ is the electromagnetic force, $\bar{\sigma}_s$ the resultant surface stress and $\bar{S}$ the surface enclosing the body.

The resultant stress on a segment of a path due to the magnetic flux density field can be broken down into its individual components namely the normal and tangential component which are calculated from the individual components of the magnetic flux density as follow

$$\sigma_t = \frac{B_n B_t}{\mu_0} \tag{2.1.2}$$

$$\sigma_n = \frac{B_n^2 - B_t^2}{2\mu_0} \tag{2.1.3}$$

where σ_t is the tangential component of the stress acting as the longitudinal tension, σ_n the normal component of the stress acting as the transverse pressure, B_n the normal component of the magnetic flux density, B_t the tangential component of the magnetic flux density and μ_0 the permeability of free space. The individual components of the magnetic flux density are obtained from the magnetic vector potential $\bar{A}$. In this work a two-dimensional model is considered therefore the magnetic vector potential only has a component in the z-direction as seen in equation (2.1.5). The magnetic flux density components are obtained as follow

$$\bar{B} = curl\bar{A} \tag{2.1.4}$$

$$= \begin{bmatrix} \bar{e}_t & \bar{e}_n & \bar{e}_z \\ \dfrac{\partial}{\partial t} & \dfrac{\partial}{\partial n} & \dfrac{\partial}{\partial z} \\ 0 & 0 & A_z \end{bmatrix} = \left(\frac{\partial}{\partial n} A_z\right)\bar{e}_t - \left(\frac{\partial}{\partial t} A_z\right)\bar{e}_n = B_t\bar{e}_t + B_n\bar{e}_n \tag{2.1.5}$$

Thus

$$B_t = \frac{\partial A_z}{\partial n} \tag{2.1.6}$$

$$B_n = -\frac{\partial A_z}{\partial t} \tag{2.1.7}$$

9

Since a two-dimensional model is considered equation (2.1.1) can be reduced to a closed line integral along a specific contour and can be represented by

$$T = \frac{1}{\mu_0} \oint_{\Gamma} r B_t B_n \cdot d\Gamma \times \ell_s \qquad (2.1.8)$$

where T is the electromagnetic torque, r is the radius of the contour Γ from the origin and ℓ_s the stack length. From this equation it is evident that only the local magnetic flux density distribution is required along the integration contour which makes the MST method probably the simplest method from a computational point of view because it makes it less complex and rather quick (Chang et al., 1989). It is also evident from equation (2.1.8) considering equation (2.1.2) that the torque of the RSM is created purely from the tangential component of the stress. In this analysis, the path of calculation is chosen to be in the middle of the air-gap and the defined path will go through elements as shown in Fig. 2.1.1 below.
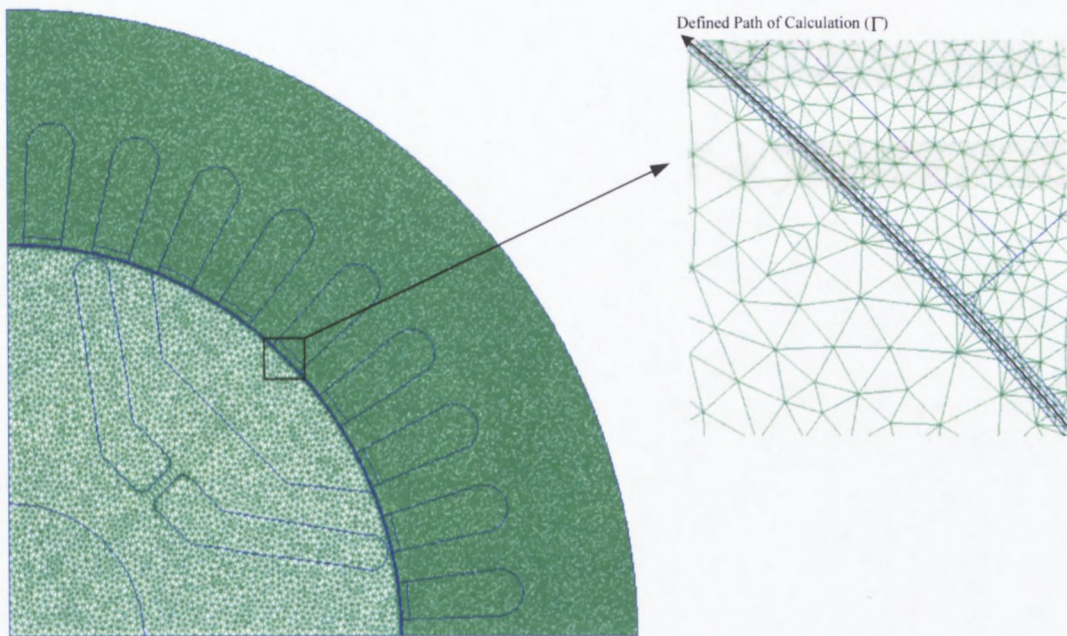
Fig. 2.1.1 Path defined in the air-gap

10

The torque as a function of the rotor position with rated sinusoidal input currents is shown in Fig. 2.1.2 below which will be compared to non-sinusoidal conditions in the following chapters.
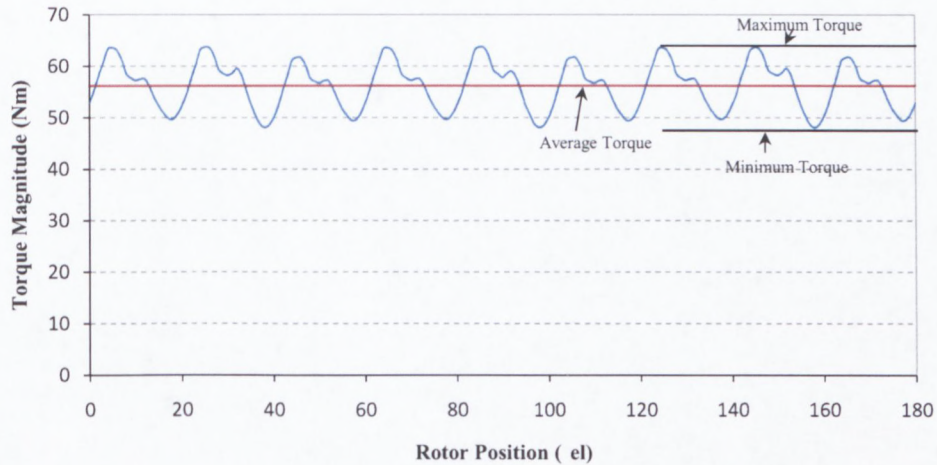
Fig. 2.1.2 Torque of the RSM fed with rated sinusoidal currents

From this graph it is evident that the torque of the RSM fluctuates periodically as the rotor rotate. This is known as torque ripple and is defined as the deviation of the minimum to the maximum from the average output torque and can be calculated according to

$$T_{ripple} = \frac{T_{max} - T_{min}}{T_{avg}} \times 100\% \tag{2.1.9}$$

where T_{max} is the maximum instantaneous torque, T_{min} the minimum instantaneous torque and T_{avg} the average torque. The torque ripple in a motor exists due to the fact that the rotor wants to be at a point of minimum energy.

11

The point of minimum energy will be explained using a two pole switched reluctance machine (SRM) for ease of understanding. The point of minimum energy exists when the rotor poles line up with the stator poles which form a path of minimum reluctance as shown in Fig. 2.1.3. As the rotor pole approaches alignment with a stator pole, the rotor is accelerated because it wants to be at a point of minimum energy. As the pole continues on its way and begins to come out of alignment with the stator pole it is "pulled backwards" or decelerated as it still wants to be at a point of minimum energy. This leads to the fluctuation of the torque.
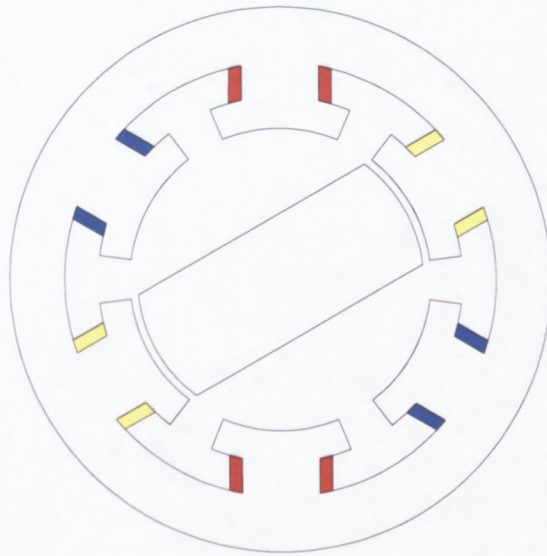
Fig. 2.1.3 SRM with rotor- and stator poles aligned

Torque ripple is unwanted as it creates uneven directional pull causing deformation of the rotor geometry which results in an uneven air gap along the inner stator circumference and mechanical vibration as well as acoustic noise (Güemes et al., 2011). It also has a detrimental effect on the mechanical parts of the machine which can lead to failure (Sturgess 1987; Turner 1981).

2.1.2 Calculation of power factor

The power factor can be calculated using different methods each depending on the preferred variables used. The method chosen for this work is the one by Kamper & Volschenk (1994) who ignores the stator resistance and the iron loss resistance given below.

$$P_f = \cos\left(\tan^{-1}\left(\frac{\sigma/\upsilon + \upsilon}{\sigma - 1}\right)\right)$$ (2.1.10)

where σ is the saliency ratio defined by L_d/L_q and υ is the ratio i_q/i_d. Equation (2.1.10) shows that the power factor is dependent on the saliency ratio and with L_q comparatively small, the power factor is sensitive to the change of its magnitude. The inductances are calculated as follows

$$L_d = \frac{\lambda_d}{i_d}$$ (2.1.11)

$$L_q = \frac{\lambda_q}{i_q}$$ (2.1.12)

where λ_d and λ_q are the d- and q-axis stator flux linkage components and i_d and i_q the d- and q-axis stator current components respectively. These stator current components or rotor quantities are obtained from the input currents using the Park's transformation matrix (Appendix A) as shown below.

$$i_d = \frac{2}{3}\left(i_R \cos(\omega t) + i_Y \cos(\omega t - 120°) + i_B \cos(\omega t + 120°)\right)$$ (2.1.13)

$$i_q = -\frac{2}{3}\left(i_R \sin(\omega t) + i_Y \sin(\omega t - 120°) + i_B \sin(\omega t + 120°)\right)$$ (2.1.14)

$$i_0 = \frac{1}{3}\left(i_R + i_Y + i_B\right)$$ (2.1.15)

where ωt is the angular velocity.

13

For symmetrical systems the zero sequence component, i_0, equals zero. Since the d- and q-axis currents are present in equation (2.1.10) it is evident that the power factor is a function of the current space phasor angle (ϕ) when looking at the following equation

$$\bar{I}_s = \sqrt{i_d^2 + i_q^2} \angle \tan^{-1}\left(\frac{i_q}{i_d}\right) \qquad (2.1.16)$$

The current space phasor and its respective components are shown in the phasor diagram below.

(a) Cross-section

(b) Space phasor diagram
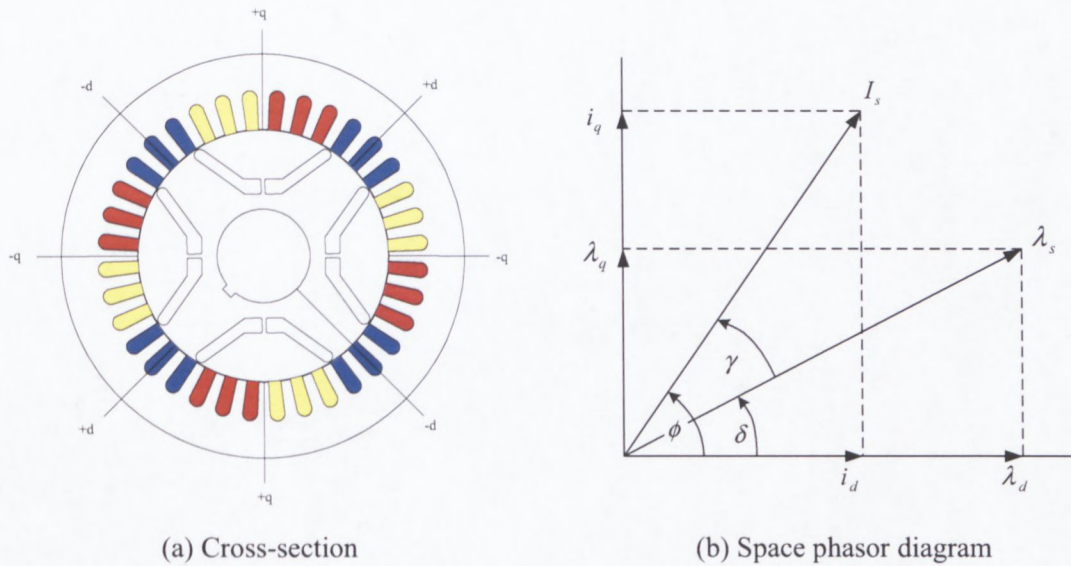
Fig. 2.1.4 Cross-sectional view of the RSM and space phasor diagram fixed to the rotor reference frame

The d- and q-axis flux linkages are the components of the flux linkage space phasor λ_s with angle δ and are shown in equations (2.1.11) & (2.1.12). These components can also be obtained from the stator quantities using Park's transformation.

14

The stator flux linkage quantities $\lambda_R, \lambda_Y, \lambda_B$ are calculated with a FE program using weighted average magnetic vector potentials, excluding end-winding linkages, given by

$$\lambda = N\ell(A_{avgGO} - A_{avgRE})$$ (2.1.17)

where N is the number of turns of the winding, ℓ is the effective length of the winding and A_{avgGO} and A_{avgRE} being the average magnetic vector potentials of the "enter" and "exit" side of the winding respectively. The method in equation (2.1.17) is established for one coil only. Therefore to calculate the stator flux linkages, the model used in this work need to be considered which consist of three windings per pole phase group (ppg) shown in Fig. 2.1.5.
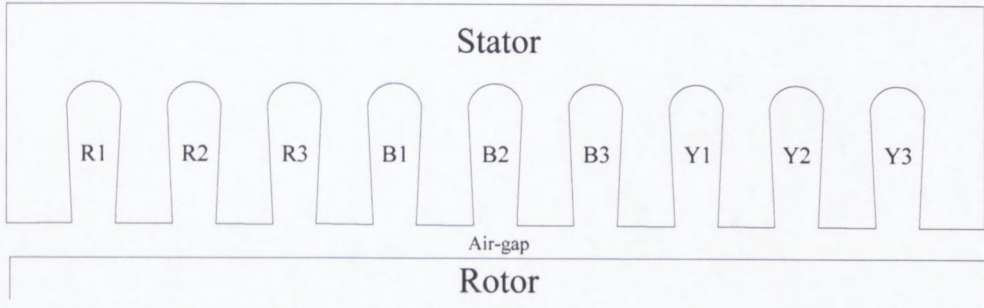
Fig. 2.1.5 Linearised cross-section of one pole of a 36 slot single layer machine

The flux linkages per ppg are calculated accordingly

$$\lambda_R = N_{ph}\ell\left[\left(A_{GOR1} - A_{RER1}\right) + \left(A_{GOR2} - A_{RER2}\right) + \left(A_{GOR3} - A_{RER3}\right)\right]$$ (2.1.18)

$$\lambda_Y = N_{ph}\ell\left[\left(A_{GOY1} - A_{REY1}\right) + \left(A_{GOY2} - A_{REY2}\right) + \left(A_{GOY3} - A_{REY3}\right)\right]$$ (2.1.19)

$$\lambda_B = N_{ph}\ell\left[\left(A_{GOB1} - A_{REB1}\right) + \left(A_{GOB2} - A_{REB2}\right) + \left(A_{GOB3} - A_{REB3}\right)\right]$$ (2.1.20)

where N_{ph} is the number of turns per phase, $A_{GOR1,GOR2,GOR3}$, $A_{GOY1,GOY2,GOY3}$, $A_{GOB1,GOB2,GOB3}$ are the weighted average magnetic vector potentials on the "enter" side of the red-, yellow- and blue phase winding and $A_{RER1,RER2,RER3}$, $A_{REY1,REY2,REY3}$, $A_{REB1,REB2,REB3}$ are the weighted average magnetic vector potentials on the "exit" side of the red-, yellow- and blue phase

15

winding. The three stator quantities are transformed into the three rotor quantities according to 、

$$\lambda_d = \frac{2}{3}\left(\lambda_R \cos(\omega t) + \lambda_Y \cos(\omega t - 120°) + \lambda_B \cos(\omega t + 120°)\right) \qquad (2.1.21)$$

$$\lambda_q = -\frac{2}{3}\left(\lambda_R \sin(\omega t) + \lambda_Y \sin(\omega t - 120°) + \lambda_B \sin(\omega t + 120°)\right) \qquad (2.1.22)$$

$$\lambda_0 = \frac{1}{3}\left(\lambda_R + \lambda_Y + \lambda_B\right) \qquad (2.1.23)$$

In this work the flux linkages are symmetrical therefore the zero sequence component, λ_0, becomes zero and can be neglected.

2.1.3 Calculation of power and efficiency

The torque of the RSM is calculated in the centre of the air-gap from the cross product between the electromagnetic force along the path in the centre of the air-gap and the radius of the path from

$$T = \vec{r} \times \vec{F} \qquad (2.1.24)$$

From this the power in the centre of the air-gap can be calculated which is in fact the output power on the shaft of the machine since the iron losses, possible bearing and windage losses, in the rotor and stator are neglected in this work because the RSM used is laminated. The output power on the shaft as a function of the rotor position can be obtained using

$$P_{out} = T\omega_n \qquad (2.1.25)$$

where $\omega_n = 2\pi n$ is the angular velocity. In this work only the copper loss is considered and calculated from

$$P_{cu} = 3I_{ph}^{2} r_s \qquad (2.1.26)$$

where P_{cu} is the total copper loss and I_{ph} the rms phase current. From equations (2.1.25 & 2.1.26) the efficiency can be calculated as

$$\eta = \frac{P_{out}}{P_{out} + P_{cu}} \times 100\% \qquad (2.1.27)$$

where the input power is equal to the losses added to the output power.

3. Machine Subjected to Fundamental Currents

The performance study of the RSM under non sinusoidal current supply is compared to the behaviour under purely fundamental current conditions. Therefore this chapter will focus on the performance of the RSM fed by fundamental sinusoidal currents only.

3.1 Torque and torque ripple

The torque of a RSM is greatly influenced by the current space phasor angle, ϕ. In this study it was found that the optimal current space phasor angle for best average torque and smallest possible torque ripple is 52.5° el. under fundamental current conditions which is shown in Fig. 3.1.1.
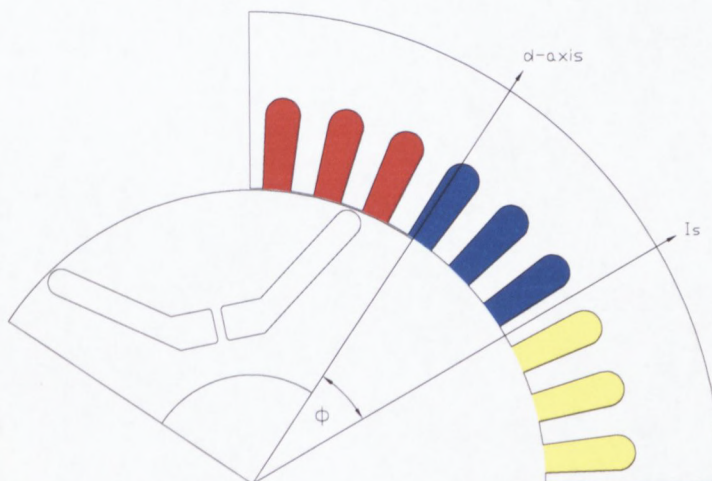
Fig. 3.1.1 Quarter RSM showing the current space phasor angle

The torque produced from fundamental currents will be referred to as fundamental torque by the author, which is shown in Fig. 3.1.2 clearly indicating fluctuations as the rotor moves.
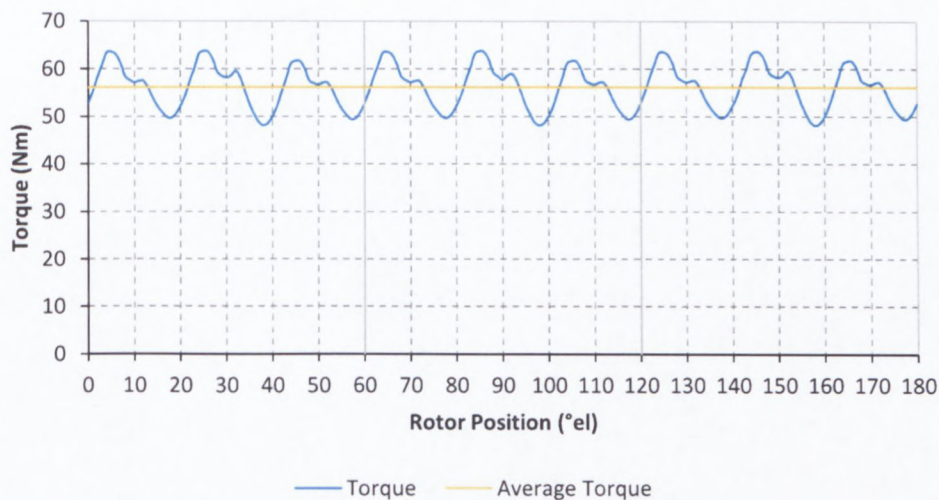
Fig. 3.1.2 Fundamental torque as a function of the rotor position

These fluctuations have a periodicity of 60° el. which is also noticeable in the fundamental three phase current waveform. This periodicity corresponds to the pitch of a ppg since it consists of 3 coils which fill 3 slots with a pitch of 20° el. each. Therefore one ppg pitch from rotor position 53° el. to 113° el. will be considered only, indicated in Fig. 3.1.3 below.
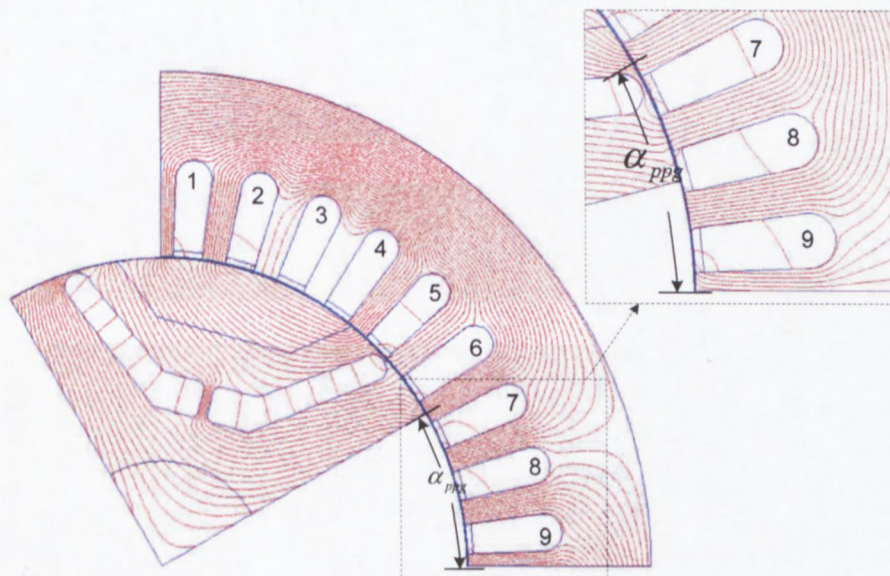
Fig. 3.1.3 Position of the d-axis at 53° el.

19

The fluctuations of the torque are due to the rotor geometry, especially the flux barrier layout which is a single flux barrier arrangement with a barrier pitch of 26° mech.

Results obtained for torque and torque ripple over a ppg pitch using the MST method when the RSM is fed with fundamental input currents only is shown in Table 3.1.1 below.

Table 3.1.1 Results

Parameter	Value
Max Torque	63.74 Nm
Min Torque	48.07 Nm
Average Torque	56.13 Nm
Torque ripple	27.92 %

3.2   Torque harmonics

The harmonic content of the output torque is obtained by performing a Fourier analysis along the path in the centre of the air-gap. Since the torque contains a dc component it will contain odd and even harmonics. The results are shown in Fig. 3.2.1.
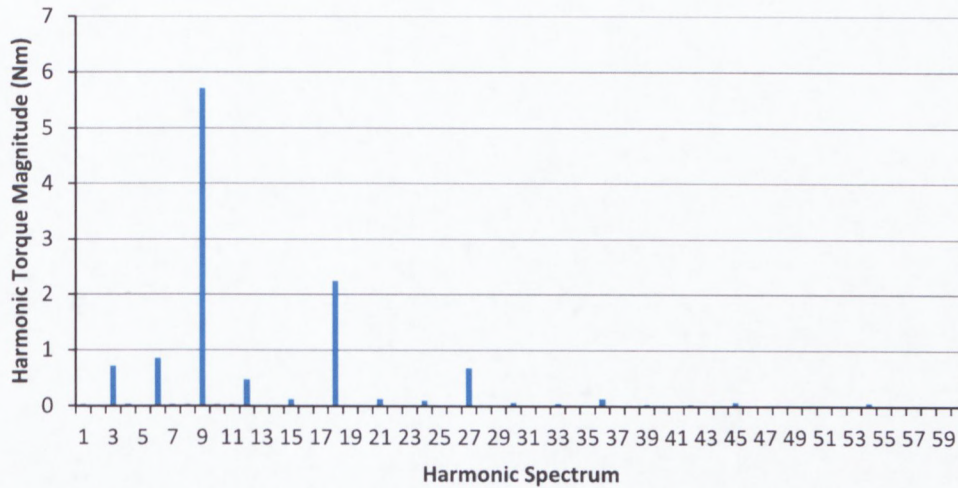
Fig. 3.2.1 Torque harmonics

From the results it is obvious that the torque produces a dominant 9th harmonic, and multiples of 9, namely the 18th and the 27th. From harmonic order 27 onwards the magnitudes are comparatively small and can be neglected. This can be ascribed to the structure of the stator which consists of 9 slots per pole (Hanekom & Voss, 2004). The 3rd, 6th and 12th harmonic are also fairly dominant.

3.3   Power factor and power

The d- and q-axis currents are constant at 13.78 A and 17.95 A as the rotor rotates as shown in Fig. 3.3.1.
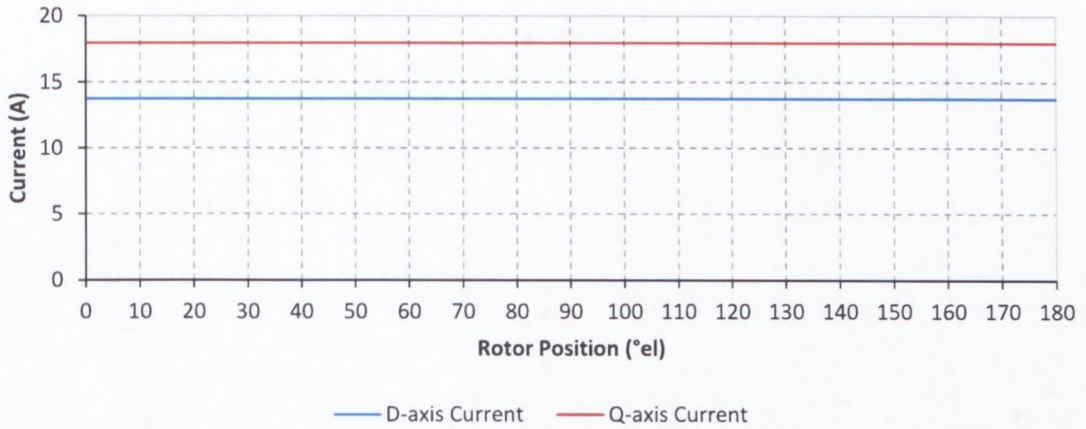
Fig. 3.3.1 D- and q-axis currents as a function of rotor position

Therefore the qd-current ratio, $v = \dfrac{i_q}{i_d}$, will be constant at 1.3. However the d- and q-axis flux linkages fluctuate due to the reluctance variation in the RSM. This causes the d- and q-axis inductances to fluctuate in the same manner as their respective flux linkages as shown in Fig.'s 3.3.2 & 3.3.3.
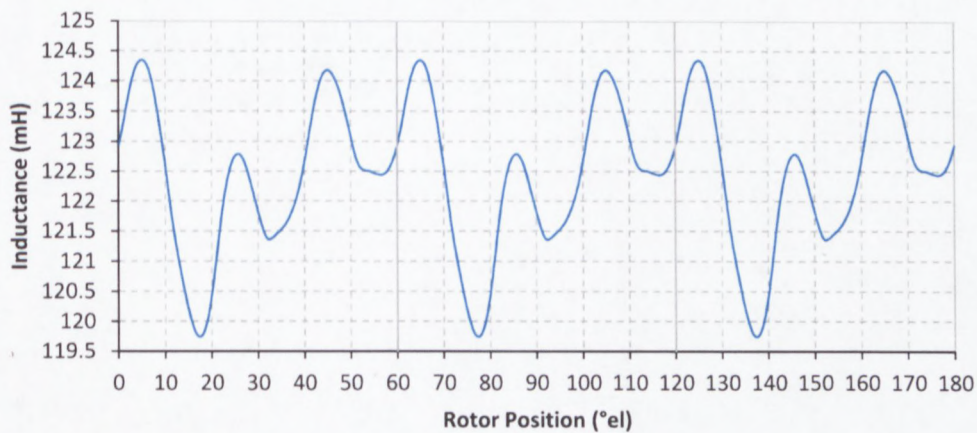
Fig. 3.3.2 D-axis inductance as a function of rotor position

22
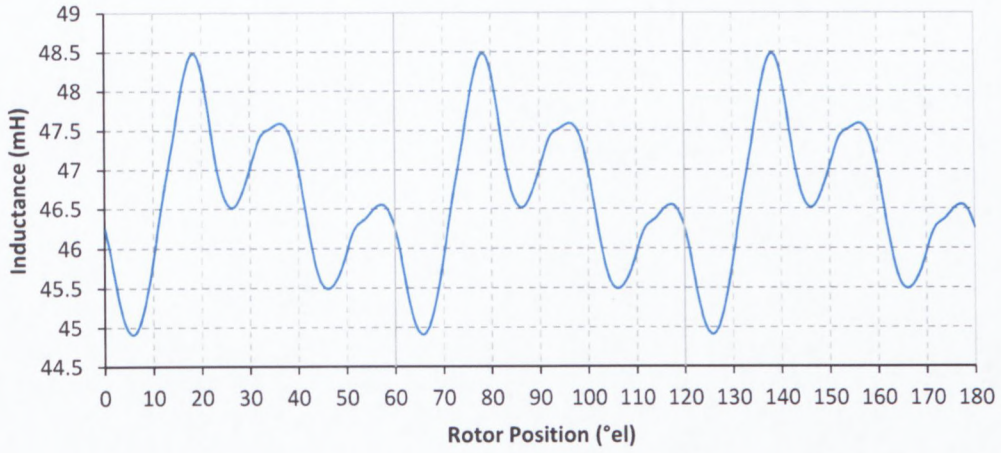
Fig. 3.3.3 Q-axis inductance as a function of rotor position

From Fig.'s 3.3.2 & 3.3.3 it is evident that when the d-axis inductance changes in one direction the q-axis inductance changes in the opposite direction. From the d- and q-axis inductance's the saliency ratio is calculated and shown as a function of the rotor position in Fig. 3.3.4, also showing a periodicity of 60° el.
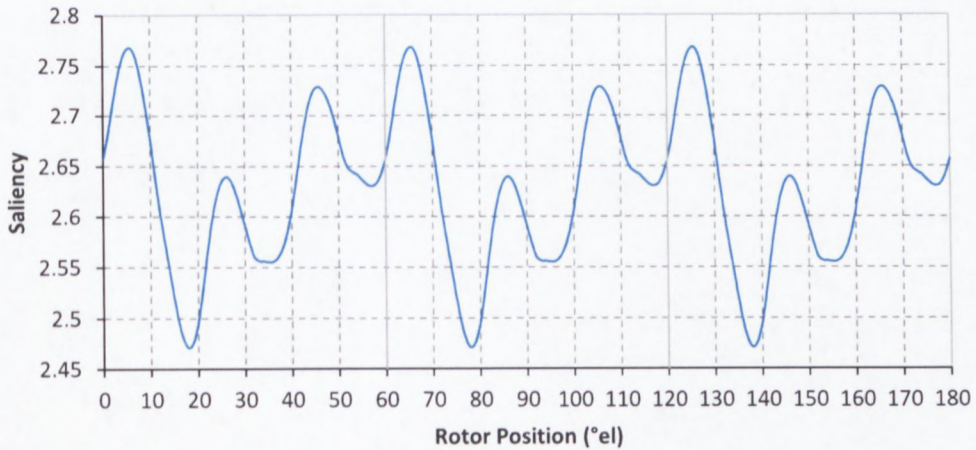
Fig. 3.3.4 Saliency ratio as a function of rotor position

With the saliency and qd-current ratio the power factor is calculated from equation (2.1.10) and is shown in Fig. 3.3.5.
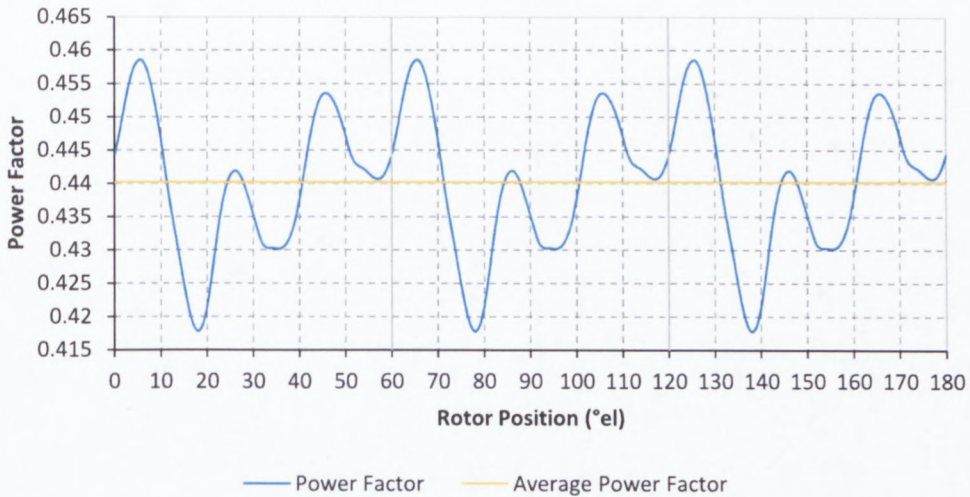
Fig. 3.3.5 Power factor as a function of rotor position

From Fig. 3.3.5 it is apparent that the average power factor is low. This is mainly due to the low average saliency ratio of the RSM calculated to be 2.63 which is due to the rotor anisotropy.

The output power on the shaft of the machine is calculated according to equation (2.1.25) and is shown in Fig. 3.3.6.
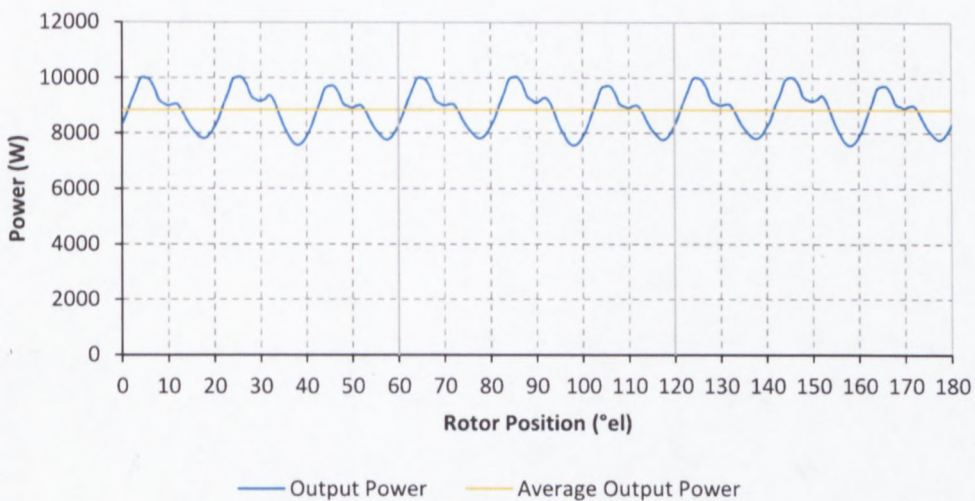
Fig. 3.3.6 Power as a function of rotor position

Results obtained for power factor and power over a ppg pitch when the RSM is fed with fundamental input currents only is shown in Table 3.3.1 below.

Table 3.3.1 Results

Parameter	Value
Average Power Factor	0.44
Max Power	10 kW
Min Power	7.6 kW
Average Power	8.8 kW

3.4   Winding losses and efficiency

The winding loss of the RSM is calculated to be 1459.2 W according to equation (2.1.26). From the output power and losses the efficiency is calculated according to equation (2.1.28) and is shown in Fig. 3.4.1.
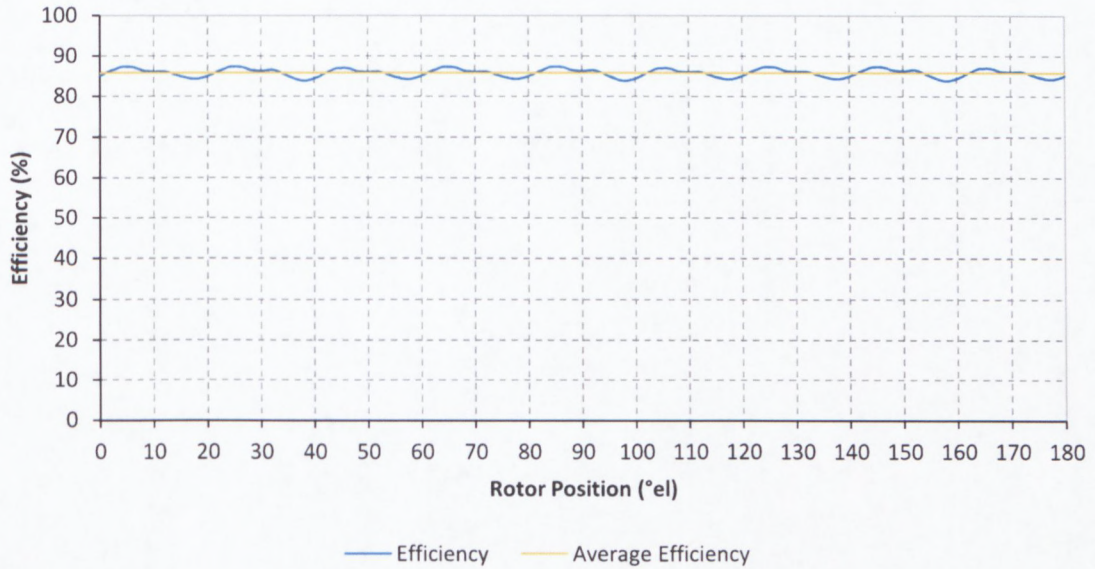
Fig. 3.4.1 Efficiency as a function of rotor position

It shows that the efficiency is fairly constant. The average efficiency of the RSM is 85.7 %.

4. Machine Subjected to Ideal Current Harmonics

This chapter will focus on the performance parameters of the RSM with the machine subjected to ideal current harmonics created by a six pulse drive added to the fundamental three phase input currents. The results will be compared to rated current performance and individual current harmonics will be removed to see the effect each harmonic has on the performance parameters. The harmonic orders created by a six pulse drive are

$$n = 6k \pm 1 \tag{4.1}$$

where $k \in N$. The highest harmonic order considered is $n = 6(4) + 1 = 25$ as higher harmonic orders are of no significance. All ideal harmonics are theoretically predicted and are calculated for each phase by

$$i_R = \frac{I}{n}\cos(n\omega t) \tag{4.2}$$

$$i_Y = \frac{I}{n}\cos(n\omega t - 120°) \tag{4.3}$$

$$i_B = \frac{I}{n}\cos(n\omega t + 120°) \tag{4.4}$$

27

The current waveform containing all the ideal harmonics (5th, 7th, 11th, 13th, 17th, 19th, 23rd and 25th) is shown in Fig. 4.1 for the three phases.
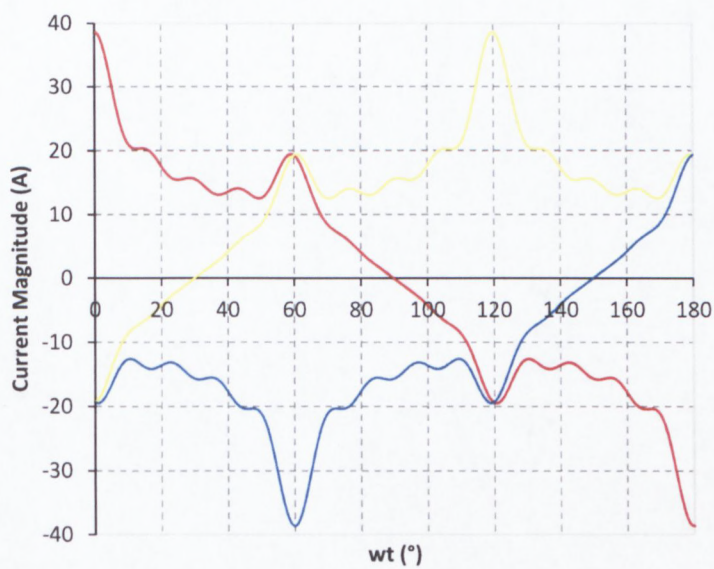
Fig. 4.1 Three phase currents containing ideal harmonics

4.1 Torque and torque ripple

The torque produced by ideal harmonic currents added will from now on be referred to as ideal torque. The total ideal torque as a function of the rotor position is shown in Fig. 4.1.1.
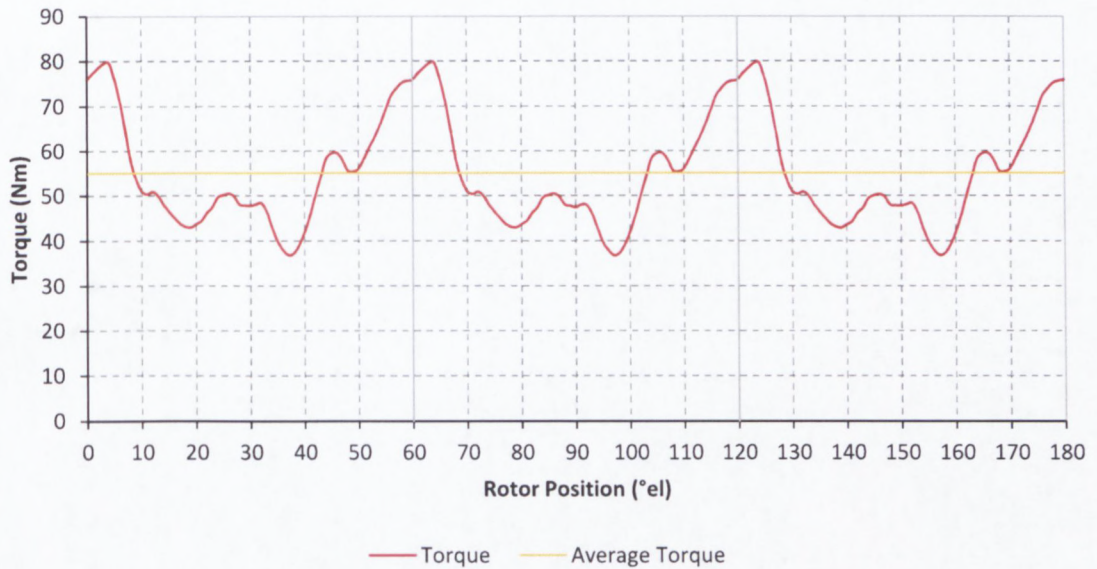
Fig. 4.1.1 Ideal torque as a function of rotor position

The graph shows that the ideal torque has a periodicity of 60° el. Comparing the ideal torque to the fundamental torque it is noticeable that their wave shapes are similar for certain rotor positions and that the ideal torque has significantly high peaks.

The ideal and fundamental torque graphs are shown in Fig. 4.1.2 for rotor positions 45° el. to 135° el. These positions were chosen to show two full peaks.
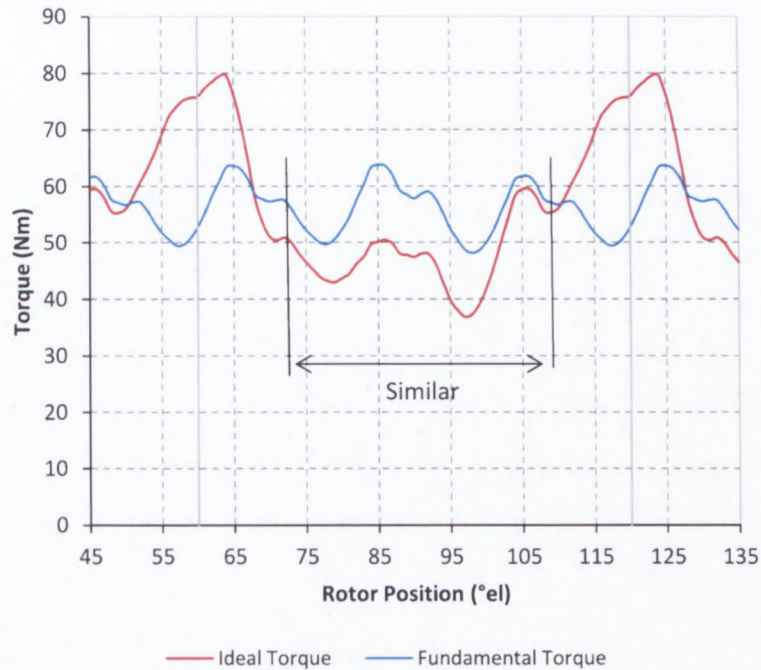
Fig. 4.1.2 Ideal- and fundamental torque as a function of rotor position

The rotor positions where the shape of the graphs is similar are from 71° el. to 109° el. as indicated in Fig. 4.1.2. From 50° el. to 64° el. the ideal torque increases drastically to an absolute maximum and its value is 24.88% higher than the absolute maximum of the fundamental torque reached at 85° el. This is the result of the ideal harmonic currents added to the fundamental which create high current peaks. These peaks occur every 60° el. and can be seen in Fig. 4.1. The average ideal torque is only 2% lower than the average fundamental torque while the torque ripple is 49.97% higher. The high torque ripple can be ascribed to the high current peaks.

The following section focuses on the ideal torque graph with individual current harmonics removed. Since the absolute maximum torque is significantly higher compared to the relative maxima, this value is noted in Table 4.1.1 as well as the average torque and torque ripple. The torque graphs with individual current harmonics removed are shown in Fig. 4.1.3.
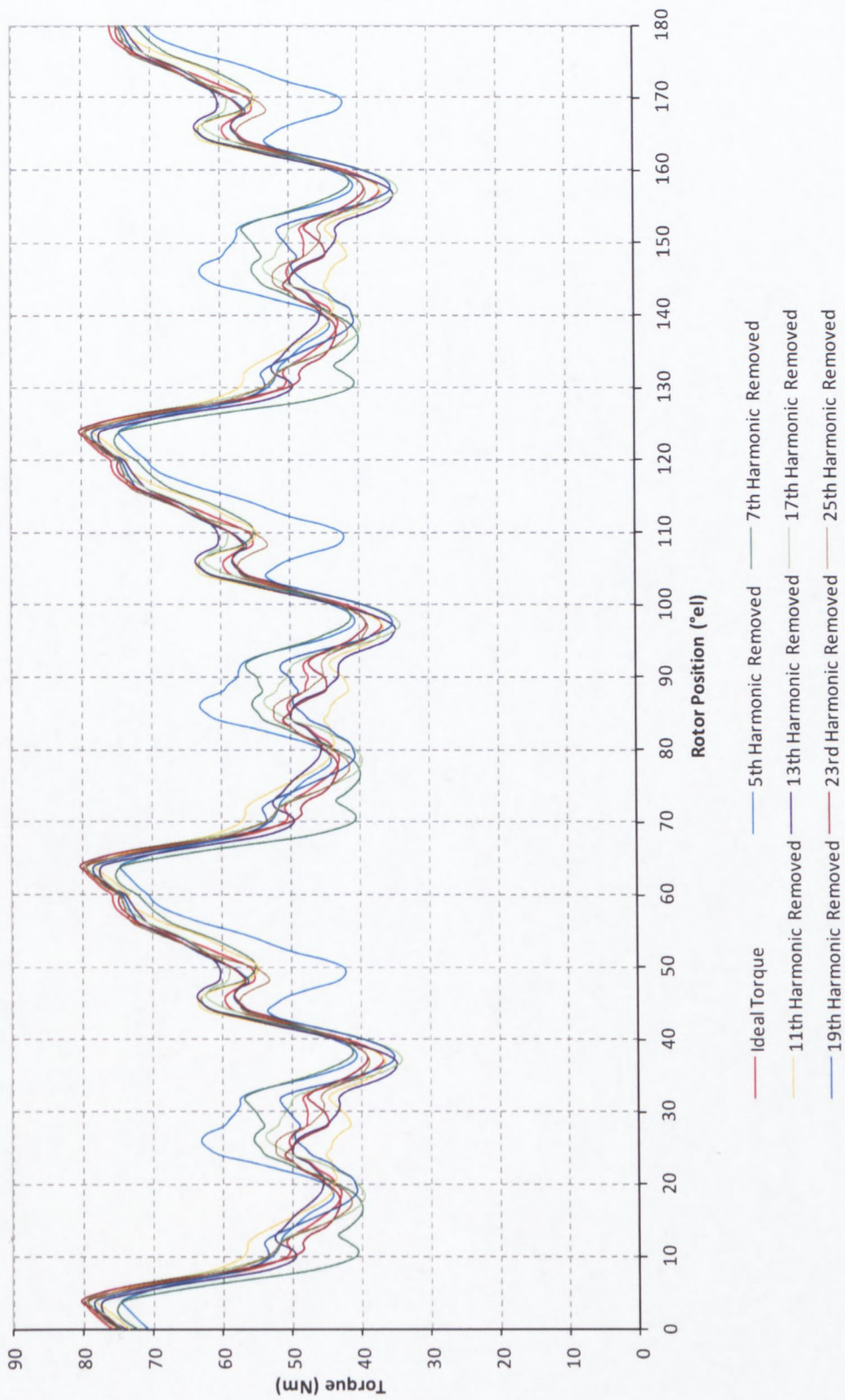
Fig. 4.1.3 Torque graphs with individual current harmonics removed

31

Table 4.1.1 Absolute maximum, average and ripple of the ideal torque when individual current harmonics is removed

	Absolute Maximum Torque (Nm)	Average Torque (Nm)	Torque ripple (%)
Ideal Torque	79.61	54.99	77.9
5th Current Harmonic Removed	74.51	54.71	61.93
7th Current Harmonic Removed	75.21	54.33	65.05
11th Current Harmonic Removed	78.4	54.71	76.64
13th Current Harmonic Removed	77.48	54.93	77.52
17th Current Harmonic Removed	79.63	55.13	82.83
19th Current Harmonic Removed	78.42	54.96	78.36
23rd Current Harmonic Removed	80.22	54.97	74.92
25th Current Harmonic Removed	79.21	54.97	73.82

From Table 4.1.1 it is evident that the 5th current harmonic has the greatest influence on the ideal torque. Without the 5th current harmonic the absolute maximum decreases by 6.4% and the torque ripple by 15.97%. Without the 17th current harmonic the average torque is the greatest at 55.13 Nm and is only 0.26% higher than the average ideal torque. This means there's only a small difference in torque with or without the 17th current harmonic.

4.2 Torque harmonics

The harmonic content of the ideal torque are compared to the harmonic content of the fundamental torque as shown in Fig. 4.2.1.
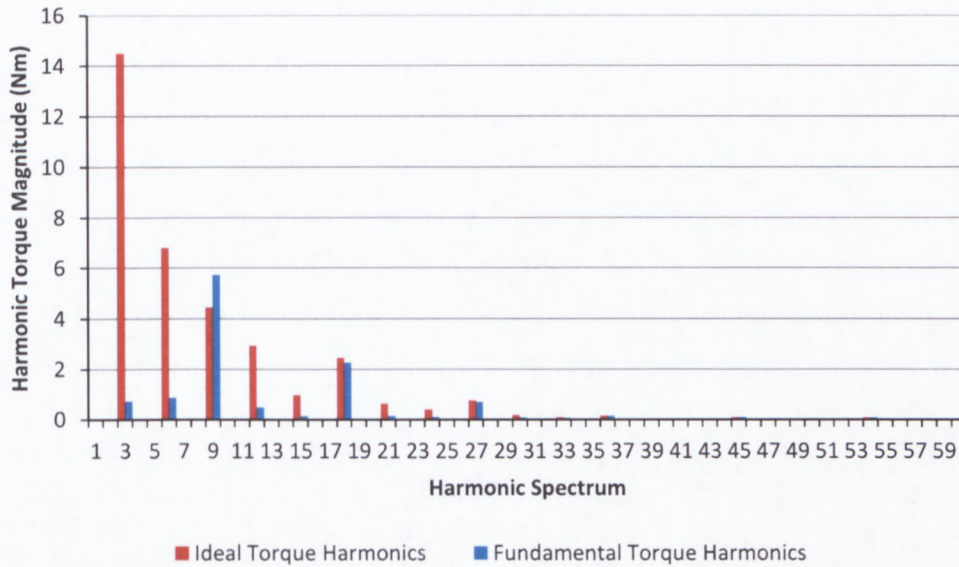
Fig. 4.2.1 Ideal- and fundamental torque harmonics

It reveals that the ideal torque consists of more dominant harmonic magnitudes than the fundamental torque. This is due to the ideal current harmonics added to the fundamental currents. The ideal torque produces a dominant 3rd harmonic, and multiples of 3, namely the 6th, 9th, 12th, 15th, 18th, 21st, 24th and 27th. The 9th harmonic order of the fundamental torque is the only harmonic greater than the ideal torque of the same order. The torque harmonics when individual current harmonics are removed is displayed in Fig. 4.2.2.
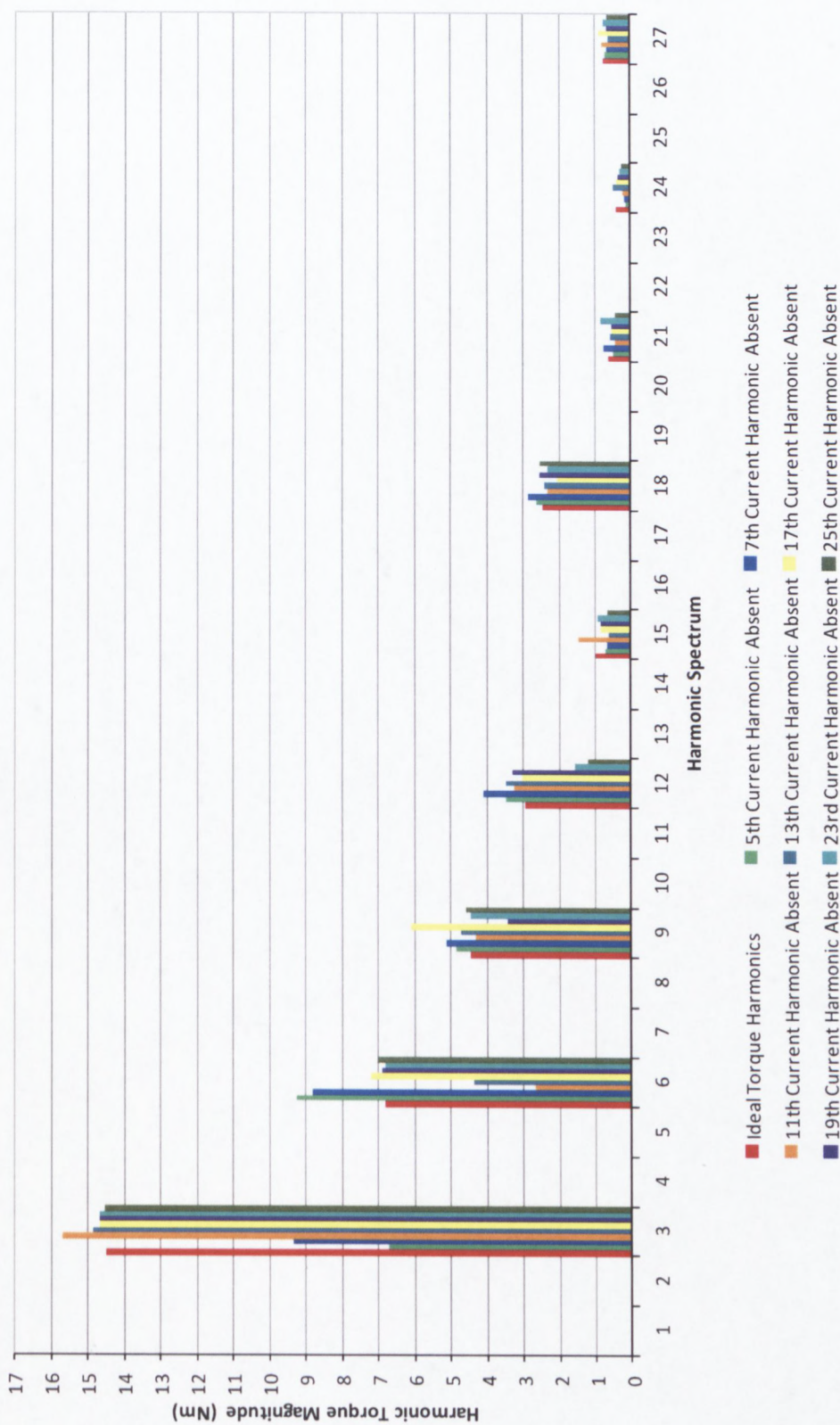
Fig. 4.2.2 Ideal torque harmonics with individual current harmonics removed

The results from Fig. 4.2.2 show that the 5th, 7th and 11th current harmonics have the greatest effect on the ideal torque. By removing the 5th current harmonic the ideal torque will have the lowest harmonic content. The 3rd ideal torque harmonic, which is the most dominant, reduces the most by 53.5% while the second most dominant harmonic, the 6th, increases the most by 35.8%. This is the main cause for the torque ripple to decrease by 15.97%. If the 7th current harmonic is removed the 3rd ideal torque harmonic reduces by 35.5% while the 6th increases by 29.2% and cause the torque ripple to decrease by 12.85%. With the 11th current harmonic absent the opposite is true. The 3rd ideal torque harmonic increased by 8.56% while the 6th decreased by 60.8%. When removing the 17th current harmonic the 9th ideal torque harmonic is greater than the 9th fundamental torque harmonic. The 9th ideal torque harmonic increased by 37.7% and is 6.8% higher than the 9th fundamental torque harmonic.

4.3   Power factor and power

The d- and q-axis currents are constant for the fundamental input currents. This is also true for the 5th current harmonic or any other harmonic considered alone because they are sinusoidal. As soon as they are superimposed the d- and q-axis currents fluctuates. The idea of the dq-transformation is somehow violated, but the results can be meaningfully interpreted. For this reason the author makes the assumption that the application of dq-transformation to quantities with harmonic content is justified. The fluctuating d- and q-axis currents cause the qd-current ratio to fluctuate as the rotor move shown in Fig. 4.3.1.
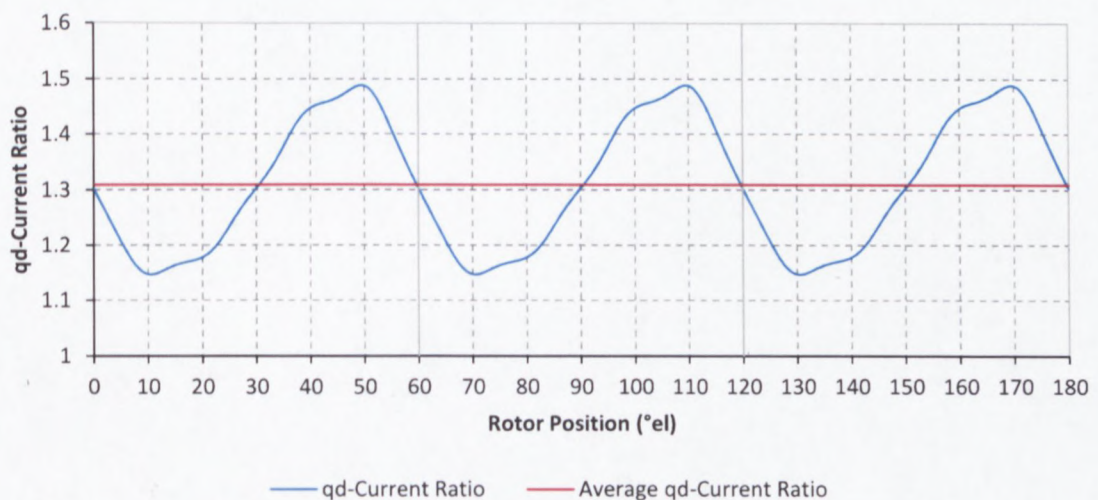
Fig. 4.3.1 qd-Current ratio as a function of rotor position

It shows that the qd-current ratio has a periodicity of 60° el. The average of the qd-current ratio is 1.3 which is equal to the constant qd-current ratio when the machine is fed with fundamental currents only. The ideal d- and q-axis flux linkages are shown in Fig.'s 4.3.2 & 4.3.3. The fundamental d- and q-axis flux linkages are also shown for easy reference.
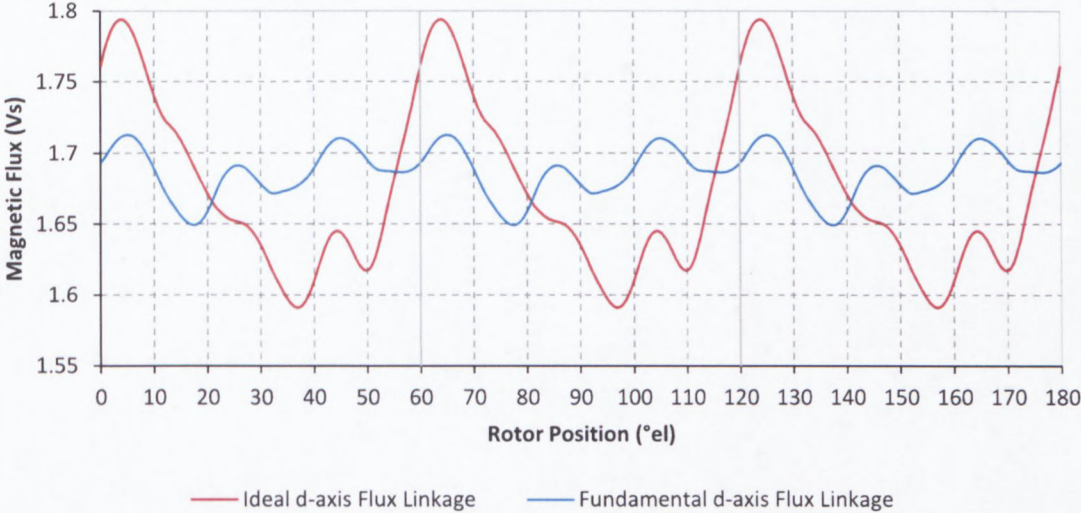
Fig. 4.3.2 Ideal and fundamental d-axis flux linkage as a function of rotor position
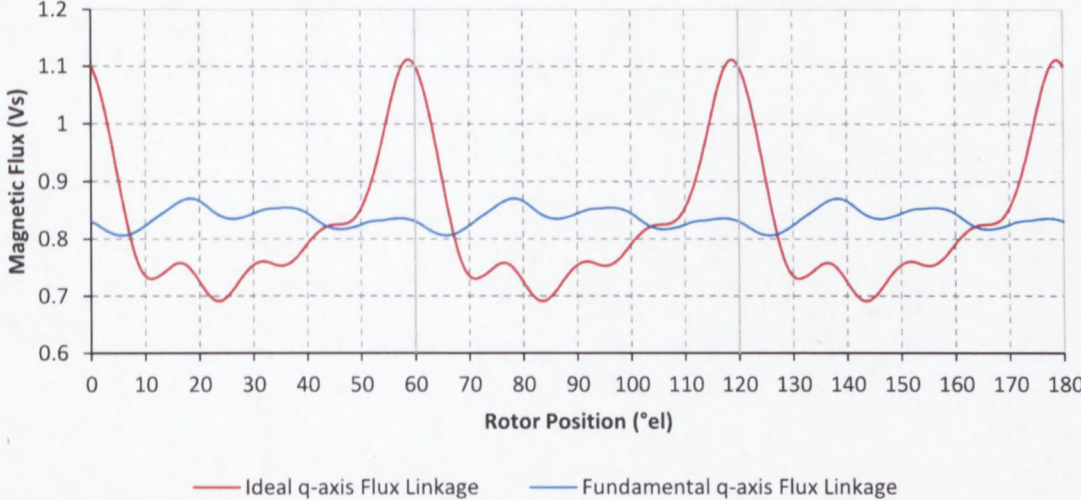
Fig. 4.3.3 Ideal and fundamental q-axis flux linkage as a function of rotor position

From the graphs it is evident that the ideal d- and q-axis flux linkages are much more distorted than the fundamental. Both graphs show a periodicity of 60° el. With the d- and q-axis flux linkages and currents the ideal d- and q-axis inductances are calculated and shown in Fig.'s 4.3.4 & 4.3.5. The fundamental d- and q-axis inductances are again shown for easy reference.
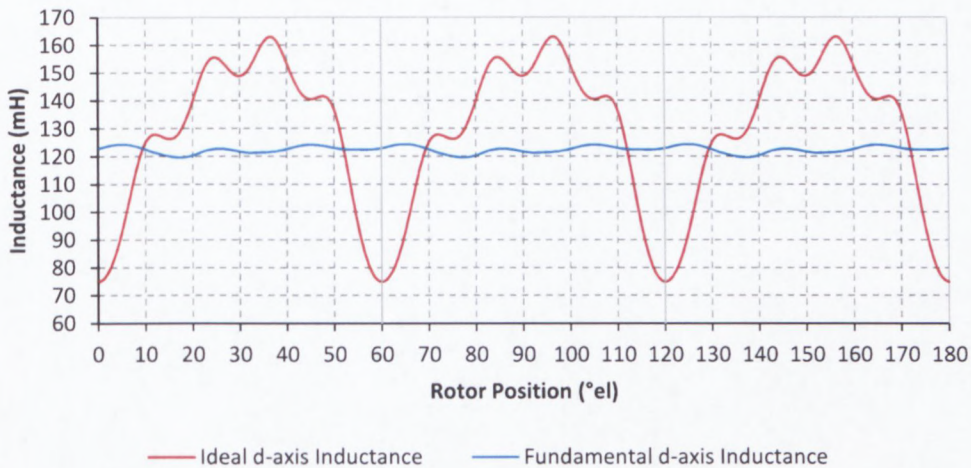
Fig. 4.3.4 Ideal and fundamental d-axis inductance as a function of rotor position
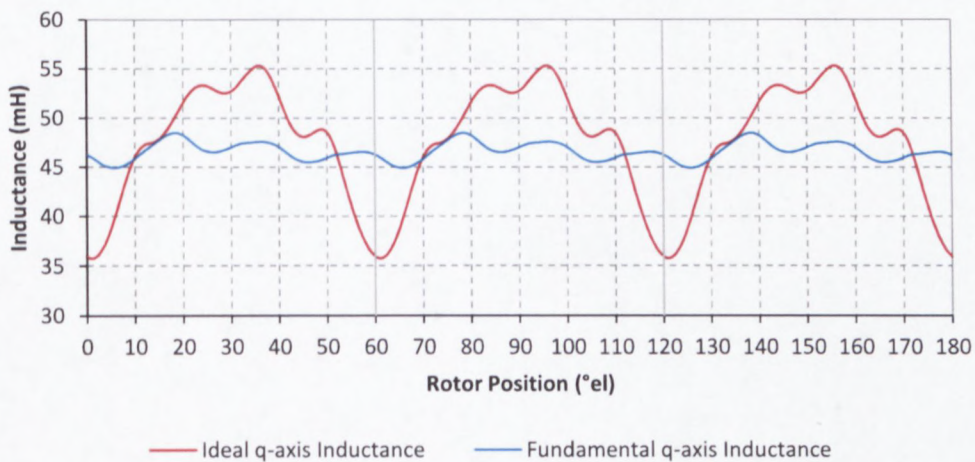
Fig. 4.3.5 Ideal and fundamental q-axis inductance as a function of rotor position

Due to the fact that the ideal d- and q-axis flux linkage's and currents fluctuate much more than the fundamental flux linkages and currents, the ideal d- and q-axis inductances fluctuate much more than the fundamental d- and q-axis inductances as shown in Fig.'s 4.3.4 & 4.3.5.

It is also noticeable that the ideal inductances have a periodicity of 60° el. From the ideal d- and q-axis inductances the ideal saliency ratio is calculated and shown in Fig. 4.3.6. The fundamental saliency ratio is shown for easy reference.
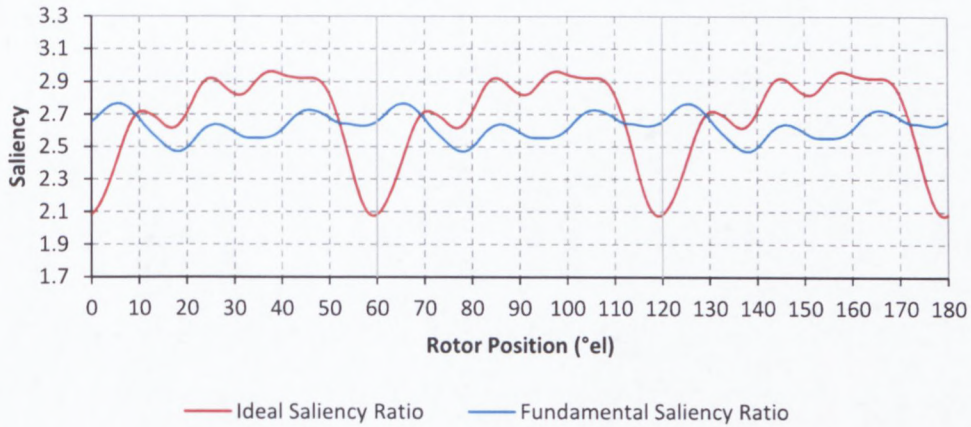
Fig. 4.3.6 Ideal and Fundamental saliency ratio as a function of rotor position

It is evident from Fig. 4.3.6 that the ideal saliency ratio has a periodicity of 60° el. and fluctuates more than the fundamental saliency ratio. With the dq-current and saliency ratio the power factor is calculated according to equation (2.1.10) and shown in Fig. 4.3.7. The fundamental power factor is shown for easy reference.
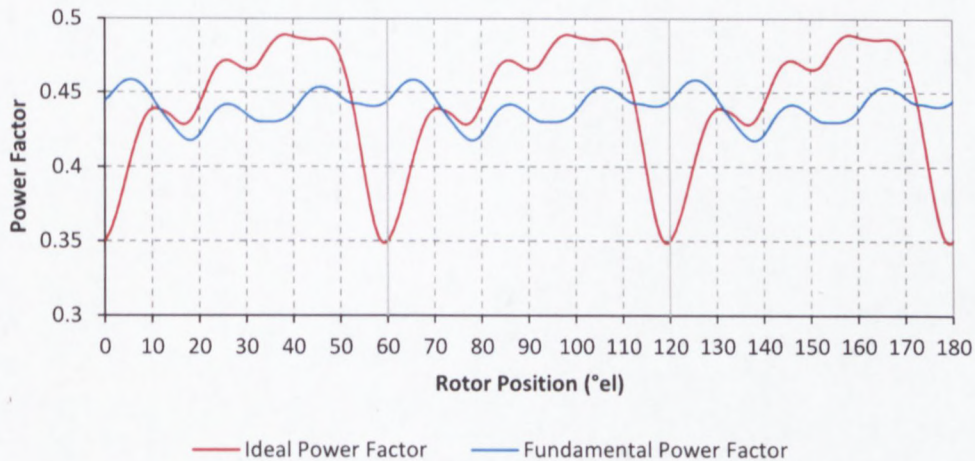
Fig. 4.3.7 Ideal and fundamental power factor as a function of rotor position

It shows that the ideal power factor has a periodicity of 60° el. and has a similar shape as the saliency ratio. Comparing the ideal power factor to the fundamental power factor it is apparent that the ideal power factor has low peaks. These absolute minimums are reached every time the ideal current reaches an absolute maximum or absolute minimum. They are also 20% lower than the absolute minimum of the fundamental power factor, which is reached at 78° el. The ideal average power factor is slightly higher than the fundamental average power factor. The average ideal power factor is 0.443 which is low and can be ascribed to the low average ideal saliency ratio of 2.68.

The following section focuses on the ideal power factor graph with individual current harmonics removed. Since the absolute minimum ideal power factor peaks are unwanted as they reduce the average power factor, they are tabulated in Table 4.3.1 as well as the average ideal power factor. The power factor graphs with individual current harmonics removed are shown in Fig. 4.3.8.
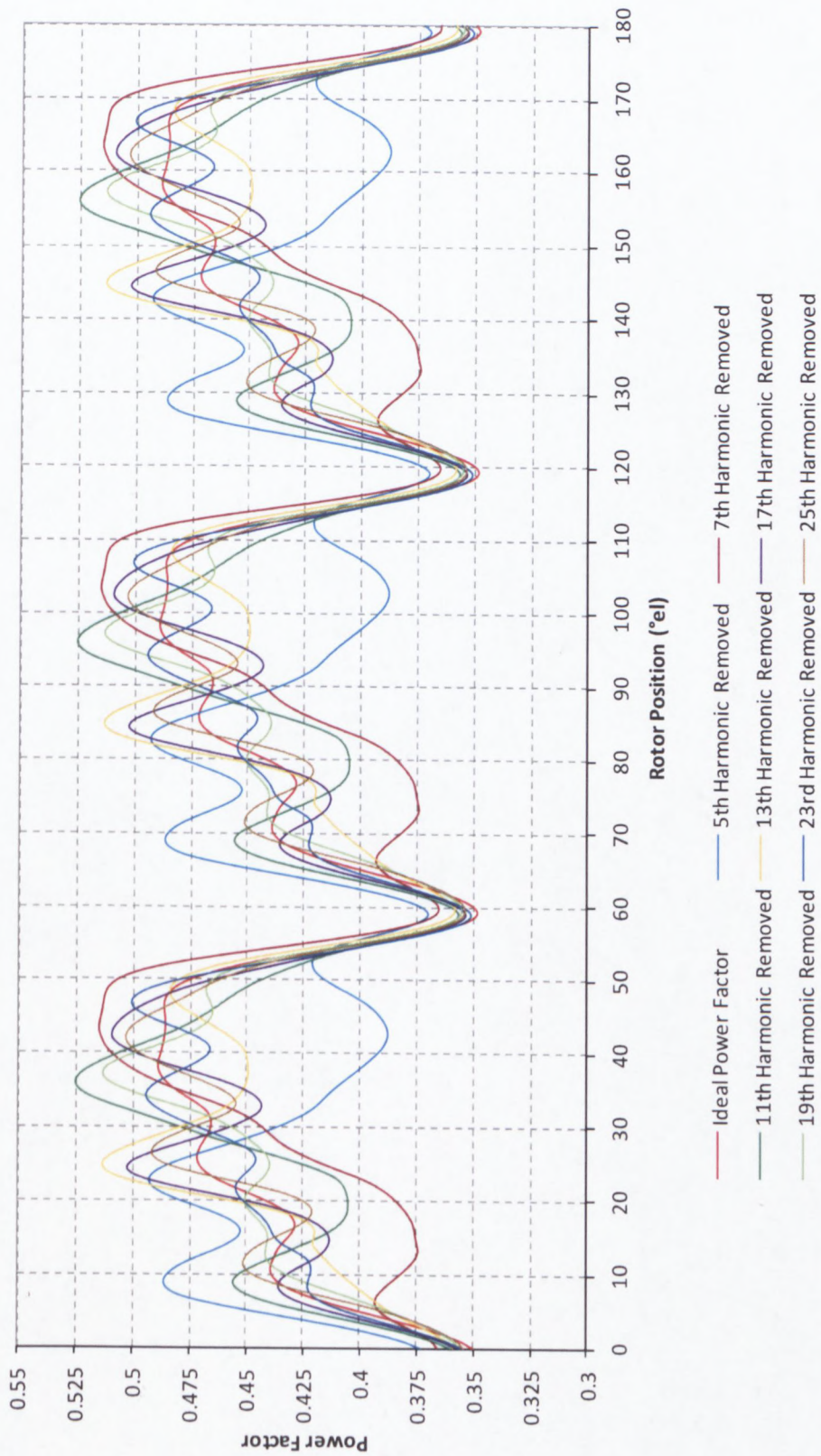
Fig. 4.3.8 Power factor graphs with individual current harmonics removed

Table 4.3.1 Absolute minimum and average ideal power factor when individual current harmonics is removed

	Absolute Minimum Power Factor	Average Power Factor
Ideal Power Factor	0.35	0.443
5th Current Harmonic Removed	0.373	0.431
7th Current Harmonic Removed	0.366	0.432
11th Current Harmonic Removed	0.34	0.441
13th Current Harmonic Removed	0.358	0.44
17th Current Harmonic Removed	0.356	0.443
19th Current Harmonic Removed	0.356	0.441
23rd Current Harmonic Removed	0.355	0.442
25th Current Harmonic Removed	0.354	0.443

From Table 4.3.1 it is evident that the 5th current harmonic has the greatest effect on the absolute minimum ideal power factor but not on the average. This is due to the fact that the 5th current harmonic is relatively low in the region between 30° el. and 50° el. Without the 5th harmonic the absolute minimum increases with 6.2%. All of the individual current harmonics have very little effect on the average ideal power factor.

The ideal output power of the machine is shown in Fig. 4.3.9. The fundamental power is also shown for easy reference.
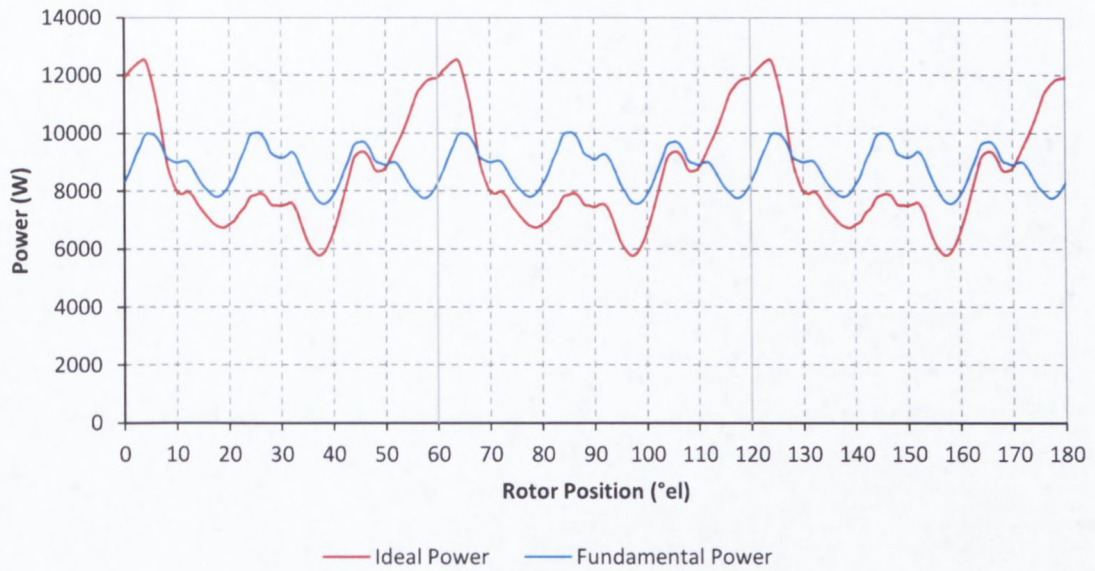
Fig. 4.3.9 Ideal and fundamental power as a function of rotor position

The power is calculated according to equation (2.1.25). Since the angular velocity is constant, the power will show the same dependency on removing current harmonics than the torque. The absolute maximum of the ideal power is 24.88% higher than the absolute maximum of the fundamental power. The ideal average power however is only 2% lower than the fundamental average power.

The following section focuses on the ideal power graph with individual current harmonics removed. The absolute maximum and average ideal power are tabulated in Table 4.3.2.

Table 4.3.2 Absolute maximum and average ideal power when individual current   harmonics
        is removed

	Absolute Maximum Power (W)	Average Power (W)
Ideal Power	12502.2	8637.52
5th Current Harmonic Removed	11701	8590.45
7th Current Harmonic Removed	11658.2	8534.04
11th Current Harmonic Removed	12311.1	8593.4
13th Current Harmonic Removed	12100.8	8627.86
17th Current Harmonic Removed	12504.8	8659.03
19th Current Harmonic Removed	12308.6	8632.66
23rd Current Harmonic Removed	12597	8634.12
25th Current Harmonic Removed	12440.2	8635.27

Table 4.3.2 shows that the 17th current harmonic removal produces the highest change in average power. The absolute maximum ideal power increases by only 0.02% and the average ideal power only by 0.25%. This means that there's only a small difference in power with or without the 17th current harmonic.

43

4.4   Winding losses and efficiency

The ideal winding loss of the RSM is calculated to be 1582.07 W according to equation (2.1.26). The ideal efficiency is shown in Fig. 4.4.1 and the fundamental efficiency calculated from equation (2.1.27) is also shown for easy reference.
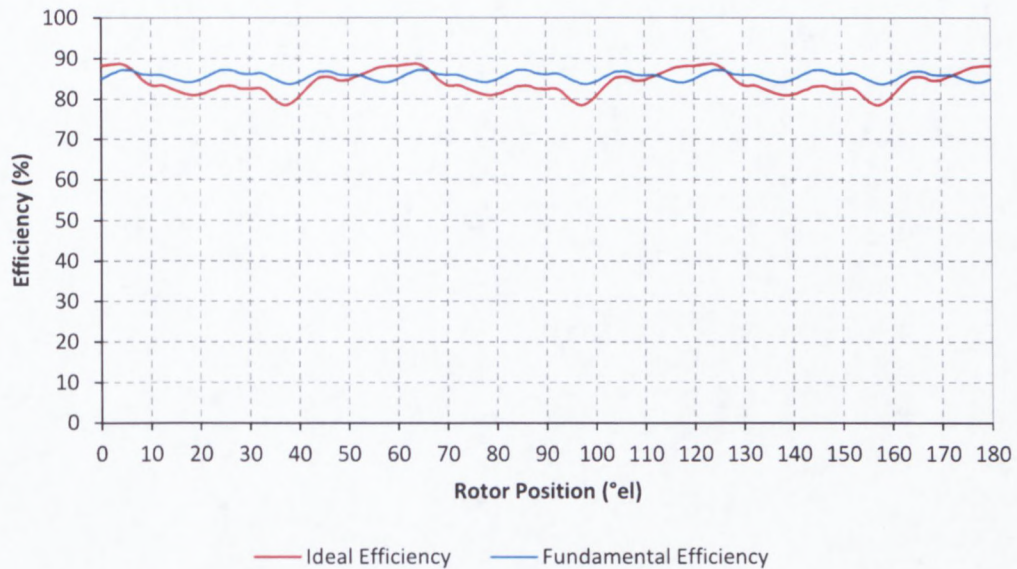
Fig. 4.4.1 Ideal and fundamental efficiency as a function of rotor position

It shows that the ideal efficiency does not differ much from the fundamental efficiency. The average ideal efficiency is only 1.7% lower than the fundamental efficiency which has a value of 84%. Since the ideal winding losses are constant the ideal efficiency graph will follow the same pattern than the ideal power graph which can also be concluded from equation (2.1.27). The average ideal efficiency graph and winding losses are tabulated in Table 4.4.1 with individual current harmonics removed.

Table 4.4.1 Ideal efficiency and winding loss when individual current harmonics is removed

	Average Efficiency (%)	Winding Losses (W)
Ideal Efficiency	84	1582.07
5th Current Harmonic Removed	84.62	1523.85
7th Current Harmonic Removed	84.2	1552.45
11th Current Harmonic Removed	84	1570.16
13th Current Harmonic Removed	84.05	1573.59
17th Current Harmonic Removed	83.99	1577.17
19th Current Harmonic Removed	84	1578.18
23rd Current Harmonic Removed	84	1579.47
25th Current Harmonic Removed	84	1579.88

From Table 4.4.1 it is noticeable that there is almost no effect on the average efficiency when the individual current harmonics are removed. The removal of the 5th current harmonic produces the highest change in winding loss reducing it by 3.68% but has very little effect on the efficiency.

45

4.5 Summary of findings

The findings of chapter 4 are summarized as follows:

- High peaks of the ideal harmonic currents cause the torque to have high peaks and therefore the torque ripple increases by 49.97%. The average ideal torque is however only 2% lower than the average fundamental torque.

- Removing the 5th current harmonic shows the best result for torque ripple as it reduces the 3rd torque harmonic (which is the most significant) by 53.5% which causes the torque ripple to decrease by 15.97%.

- The ideal current harmonics have very little effect on the average power factor and power. The power factor increased by 0.68% while the power decreased by 2%.

- The ideal current harmonics have very little effect on the efficiency since the 5th current harmonic reduces the copper loss by 3.8% (which is the highest individual contribution).

5. Machine Subjected to Published Current Harmonics

This chapter will focus on the performance parameters of the RSM with the machine subjected to published current harmonics created by a six pulse drive added to the fundamental three phase input currents. The results will be compared to rated current performance and individual current harmonics will be removed to see the effect each harmonic has on the performance parameters. The dominant published harmonic orders created by a six pulse drive are given as a percentage of the fundamental current magnitude as tabulated in Table 5.1. The angles indicated represent the phase shift with respect to the fundamental.

Table 5.1 Published current harmonic data

Harmonic Order	Percentage of Fundamental (%)	Angle (° el)
5th	23.52	111
7th	6.08	109
11th	4.57	-158
13th	4.2	-178
17th	1.8	-94
19th	1.37	-92
23rd	0.75	-70
25th	0.56	-70

The current waveform containing all the published harmonics (5th, 7th, 11th, 13th, 17th, 19th, 23rd and 25th) is shown in Fig. 5.1 for the three phases.
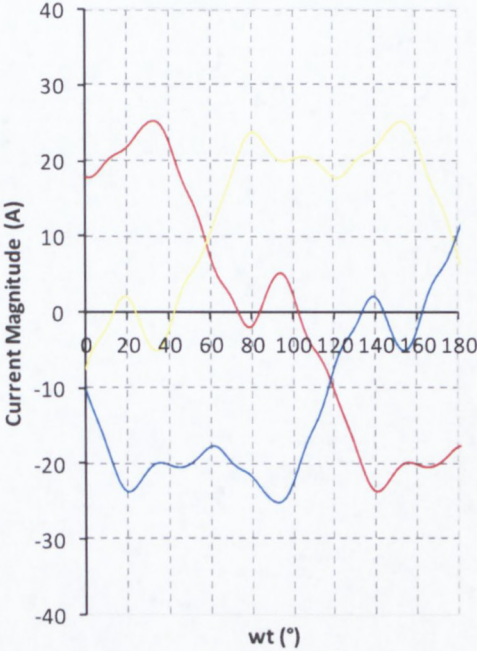
Fig. 5.1 Three phase currents containing published harmonics

5.1 Torque and torque ripple

The torque produced by published harmonic currents added will from now on be referred to as published torque. The total published torque as a function of the rotor position is shown in Fig. 5.1.1 and reveals again a periodicity of 60° el.
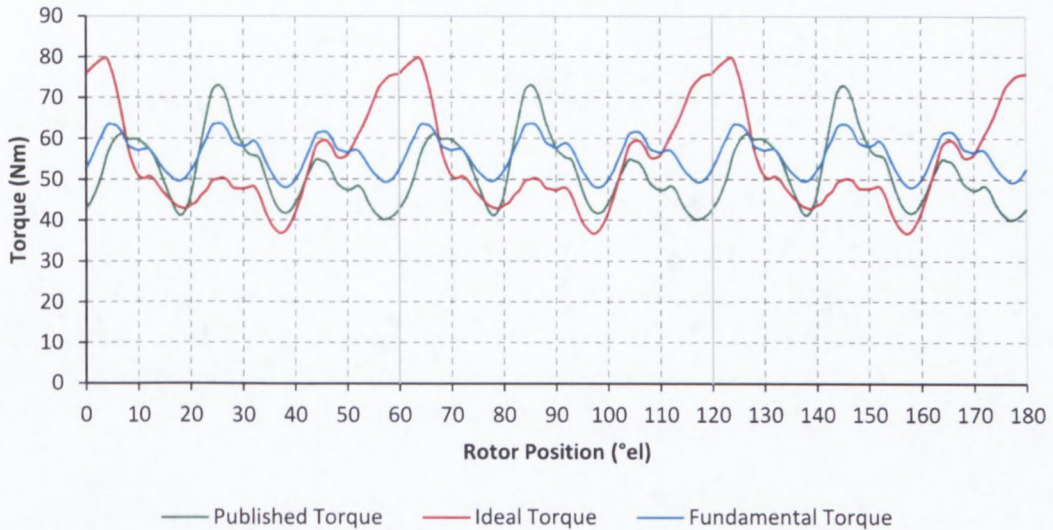
Fig. 5.1.1 Published, ideal and fundamental torque as a function of rotor position

Comparing the published torque to the fundamental torque it can be seen that their wave shapes follow a similar pattern and that the published torque peaks are not as high as the ideal torque peaks. This is due to the published harmonic currents, shown in Fig. 5.1, not having very high peaks like the ideal harmonic currents.

Considering rotor positions 60° el. to 120° el. it is evident that the published torque increases from 81° el. to 85° el. where it reaches an absolute maximum value of 73 Nm. This absolute maximum is 15.25% higher than the absolute maximum of the fundamental torque and 8.28% lower than the absolute maximum of the ideal torque reached at 64° el. This results in the published torque having a lower torque ripple than the ideal torque. The published torque ripple is 35.04% higher than the fundamental and 14.93% lower than the ideal torque ripple while the average published torque is only 7.16% lower than the fundamental and 5.27% lower than the ideal. This concludes that ideal current harmonics cause the torque ripple to increase more than published harmonic currents.

49

The following section focuses on the published torque graph with individual current harmonics removed. The absolute maximum, average and torque ripple are noted in Table 5.1.1. The torque graphs with individual current harmonics removed are shown in Fig. 5.1.2.
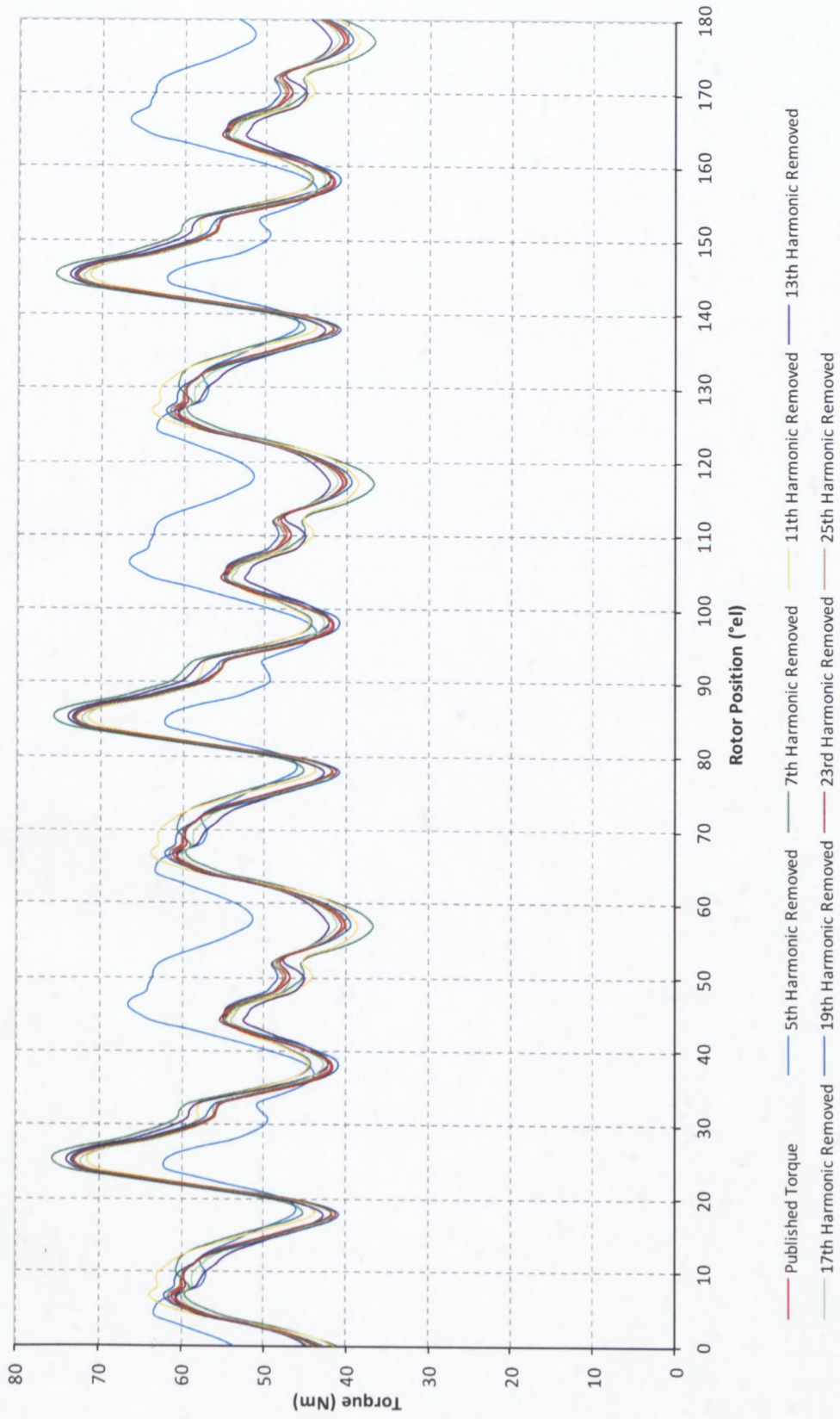
Fig. 5.1.2 Torque graphs with individual current harmonics removed

51

Table 5.1.1 Published torque when individual current harmonics is removed

	Absolute Maximum Torque (Nm)	Average Torque (Nm)	Torque ripple (%)
Published Torque	73	52.09	62.97
5th Current Harmonic Removed	62.1	55.45	40.84
7th Current Harmonic Removed	75.46	52.86	73.3
11th Current Harmonic Removed	71.3	52.51	62.31
13th Current Harmonic Removed	73.73	52.15	60.72
17th Current Harmonic Removed	72.35	52.01	59.86
19th Current Harmonic Removed	73.19	52.13	64.55
23rd Current Harmonic Removed	73.09	52.12	62.45
25th Current Harmonic Removed	73.07	52.11	63.44

Table 5.1.1 shows that the 5th current harmonic again has the greatest influence on the published torque which is visible in Fig. 5.1.2. Without the 5th current harmonic the absolute maximum decreases by 14.93%. This causes the torque ripple to decrease by 22.13%. The average published torque is also the greatest without the 5th current harmonic with a value of 55.45 Nm. This is only 6.45% higher than with the 5th included. All the current harmonics except the 5th have minor effects on the published torque. This is due to the high 5th harmonic current magnitude compared to the rest of the harmonic currents. The published torque without the 5th has a slight resemblance to the fundamental torque graph.

5.2   Torque harmonics

In this section the harmonic content of the published torque are compared to the harmonic content of the fundamental and ideal torque shown in Fig. 5.2.1.
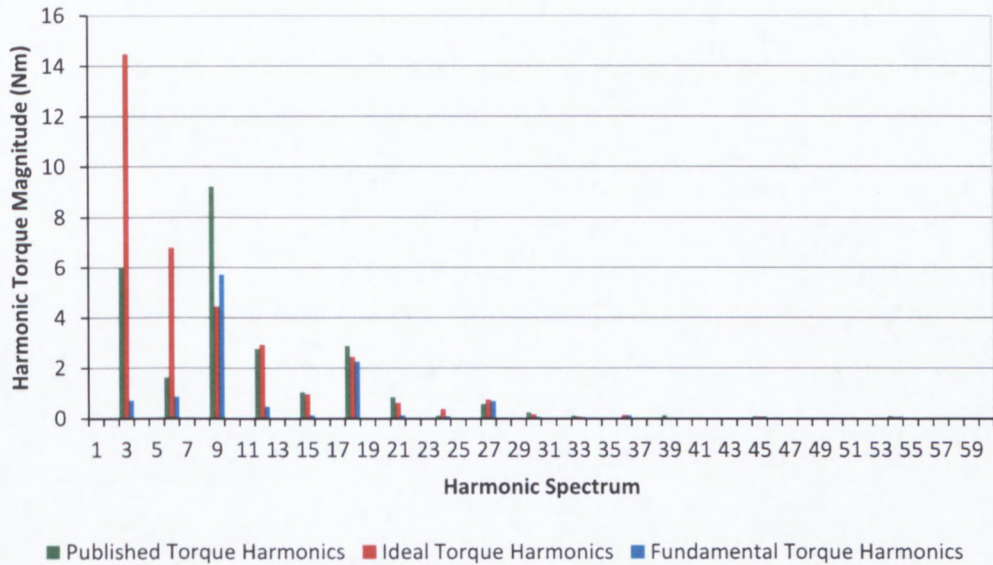
Fig. 5.2.1 Published, ideal and fundamental torque harmonics

It reveals that the published torque produces the same most dominant harmonic as the fundamental torque namely the 9th. This (published) torque harmonic increased by 60.8% compared to the 9th fundamental torque harmonic and by 107.4% compared to the 9th ideal torque harmonic. The dominant 9th published torque harmonic can be ascribed to the similar wave shapes of the published and fundamental torque. Other dominant published torque harmonics are the 3rd and multiples of 3, namely the 6th, 12th, 15th, 18th, 21st, 24th and 27th.

The 3rd published torque harmonic decreased by 58.35% compared to the 3rd ideal torque harmonic while the 6th decreased by 76.26%. This resulted in the torque ripple to decrease by 14.93% compared to the ideal torque ripple. The effect on the published torque harmonics when individual current harmonics are removed is shown in Fig. 5.2.2.
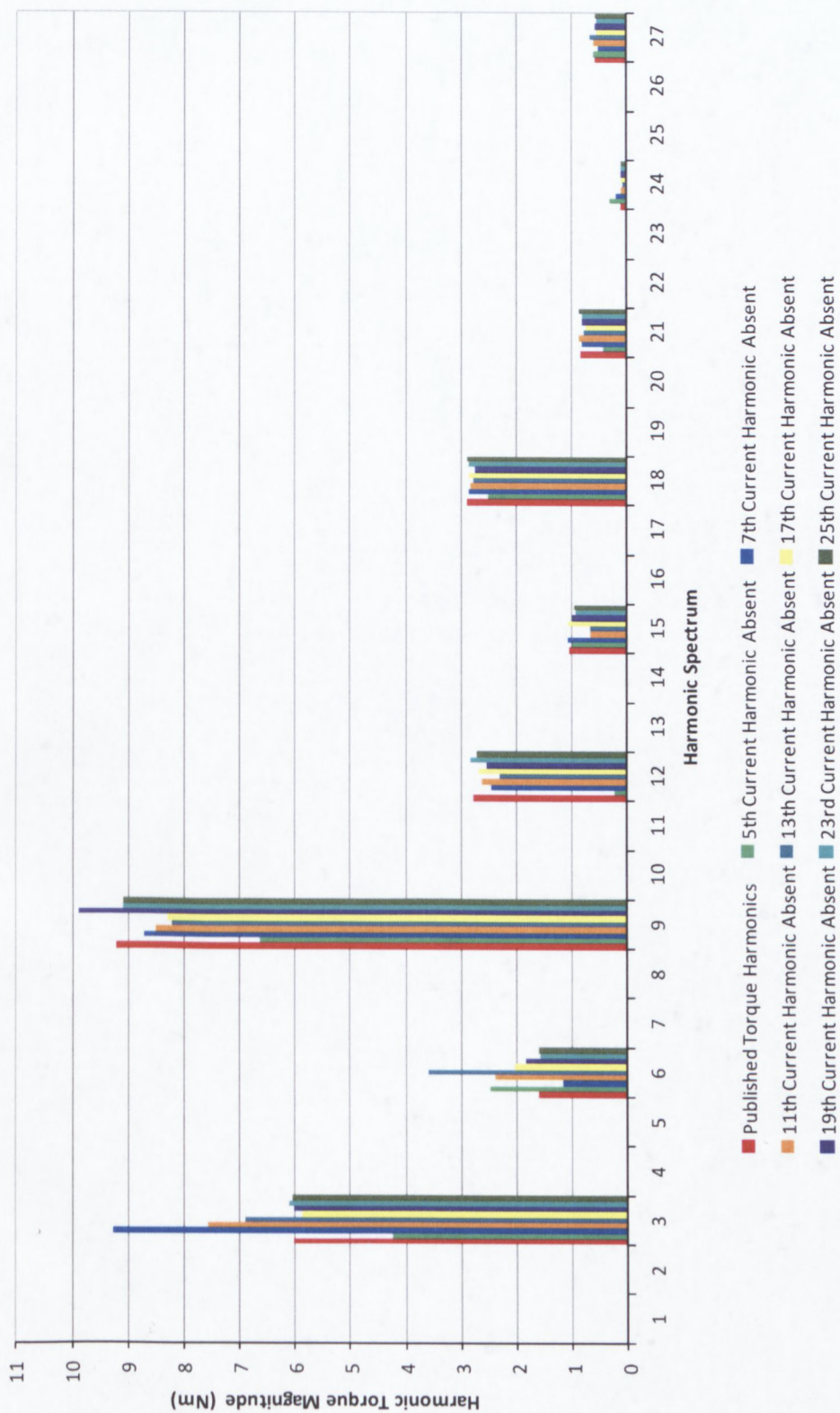
Fig. 5.2.2 Published torque harmonics with individual current harmonics removed

Results from Fig. 5.2.2 show by removing the 5th current harmonic the published torque has the lowest harmonic content. The 9th torque harmonic, which is the most dominant, reduces by 27.8% while the 3rd torque harmonic, which is the second most dominant harmonic, decreases by 29.6%. This causes the torque ripple to decrease by 22.13%. If the 7th current harmonic is removed the 3rd published torque harmonic increase by 53.72%. This causes the torque ripple to increase by 10.33% as shown in Table 5.1.1.

5.3   Power factor and power

When the machine is fed with published harmonic currents the d- and q-axis currents fluctuate as well. This causes the qd-current ratio to fluctuate as the rotor rotates as shown in Fig. 5.3.1.
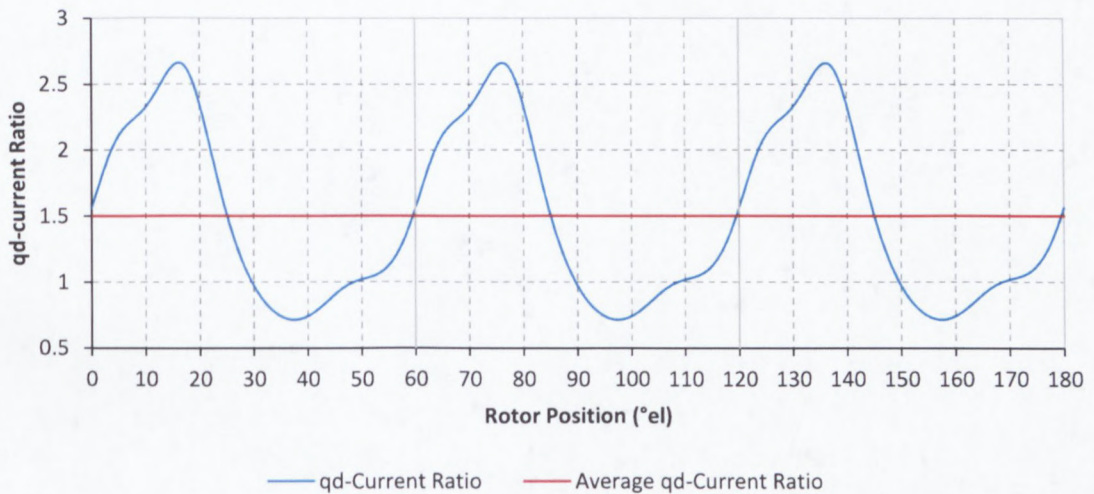
Fig. 5.3.1 qd-Current ratio as a function of rotor position

It shows that the qd-current ratio also has a periodicity of 60° el. The average of the published qd-current ratio is 1.5 which is 15.39% higher than both, the ideal qd-current ratio and the constant qd-current ratio when the machine is fed with fundamental currents only. If the average qd-current ratio increases it enhances the power factor but due to the small change this effect is minute.

The published d- and q-axis flux linkages are shown in Fig.'s 5.3.2 & 5.3.3. The ideal and fundamental d- and q-axis flux linkages are also shown for easy reference.
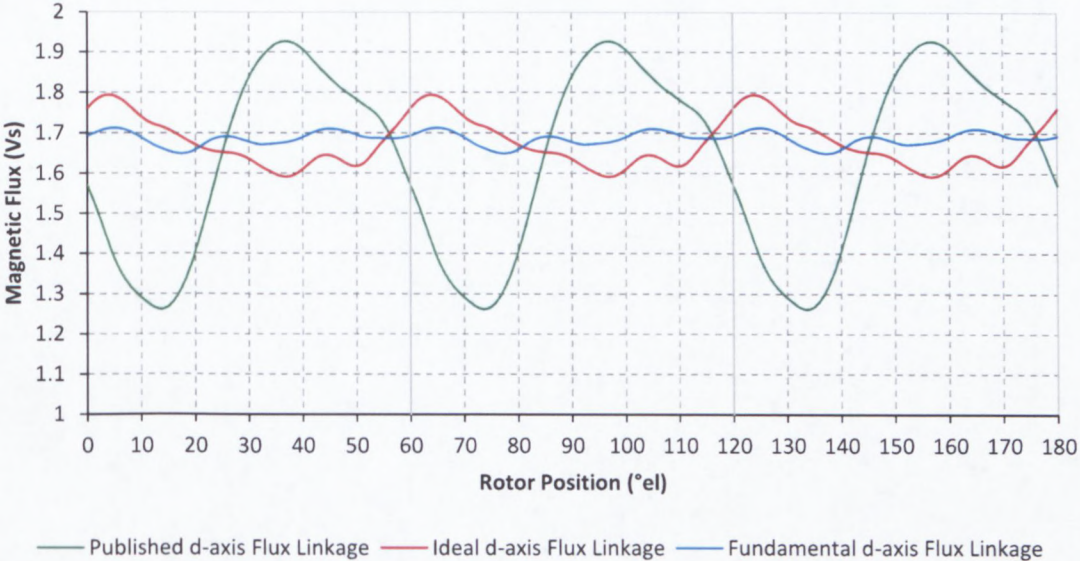
Fig. 5.3.2 Published, ideal and fundamental d-axis flux linkages as a function of rotor position
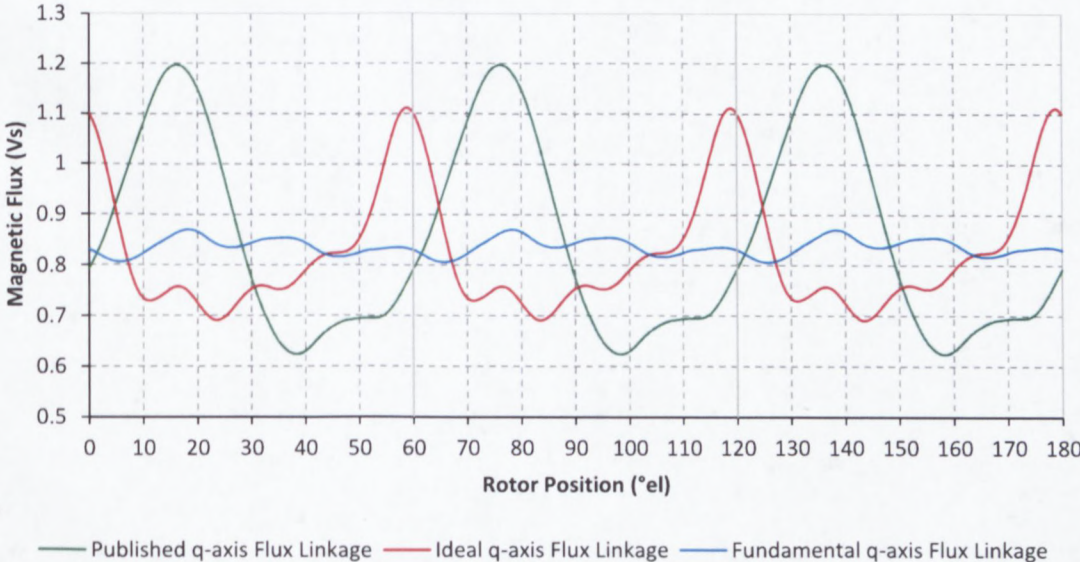
Fig. 5.3.3 Published, ideal and fundamental q-axis flux linkages as a function of rotor position

The graphs show that the published d- and q-axis flux linkages are even more distorted than the ideal and fundamental. Both graphs show a periodicity of 60° el. With the d- and q-axis flux linkages and currents the published d- and q-axis inductances are calculated and shown in Fig.'s 5.3.4 & 5.3.5. The ideal and fundamental d- and q-axis inductances are again shown for easy reference.
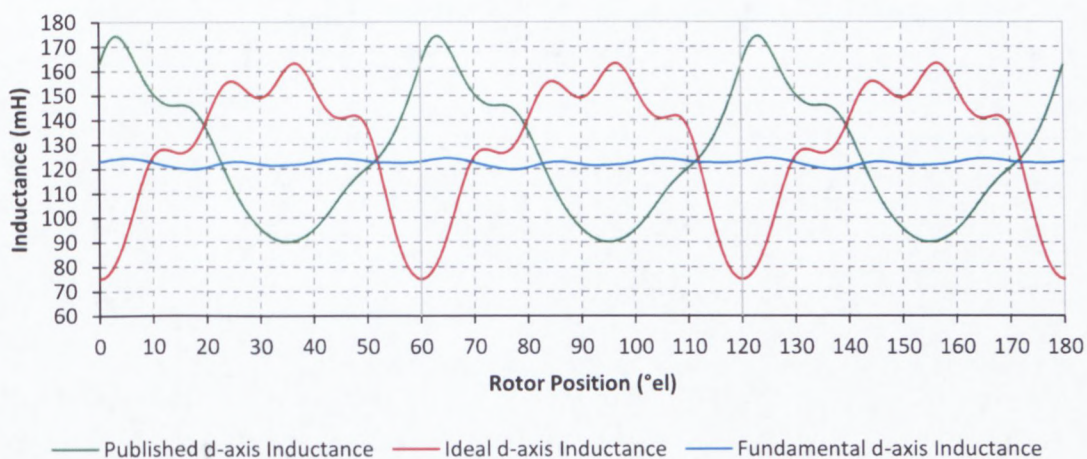
Fig. 5.3.4 Published, ideal and fundamental d-axis inductance as a function of rotor position
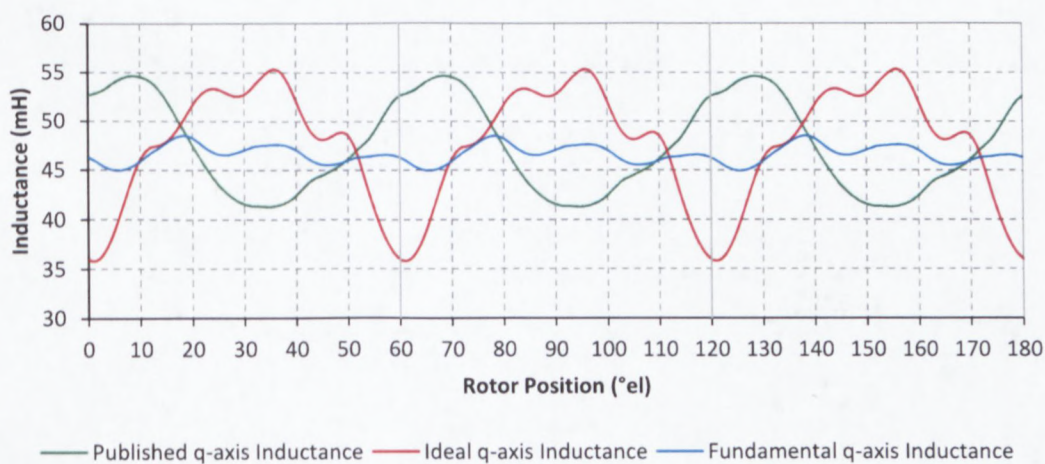
Fig. 5.3.5 Published, ideal and fundamental q-axis inductance as a function of rotor position

The fluctuating d- and q-axis published flux linkages and currents cause the d- and q-axis published inductances to fluctuate much more than the fundamental shown in Fig.'s 5.3.4 & 5.3.5. It is also noticeable that the published inductances have a periodicity of 60° el. From the published d- and q-axis inductances the published saliency ratio is calculated and shown in Fig. 5.3.6. The ideal and fundamental saliency ratio is shown for easy reference.
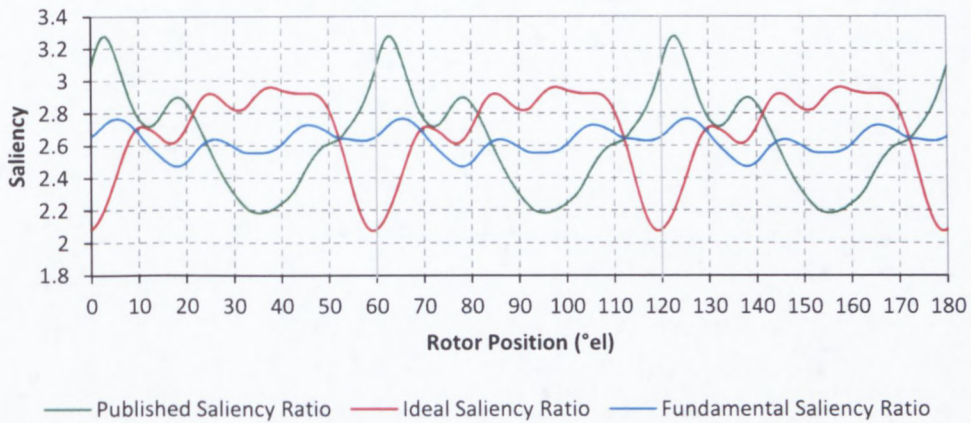
Fig. 5.3.6 Published, ideal and fundamental saliency ratio as a function of rotor position

It is evident from Fig. 4.3.6 that the published saliency ratio has a periodicity of 60° el. The average published saliency ratio is 2.65 which are 1.12% lower than the ideal and 0.76% higher than the fundamental saliency ratio.

With the dq-current and saliency ratio the published power factor is calculated according to equation (2.1.10) and shown in Fig. 5.3.7. The ideal and fundamental power factor is shown for easy reference.

Fig. 5.3.7 Published, ideal and fundamental power factor as a function of rotor position

The graphs show that the published power factor has a periodicity of 60° el. and again has a similar wave pattern as the saliency ratio. Comparing the published power factor to the ideal and fundamental power factor, it is apparent that the published power factor has the lowest peaks. The absolute minima are due to the low saliency and qd-current ratios at the respective rotor positions and are unwanted as it reduces the average published power factor. The published absolute minimum is 15% lower than the ideal absolute minimum and 35% lower than the fundamental absolute minimum power factor. The average published power factor is a little lower than the ideal and fundamental average power factor's with a value of 0.418 and can be ascribed to the low average published saliency ratio of 2.65. This concludes that the published harmonic currents have a slight negative effect on the power factor while the ideal harmonic currents almost have no effect.

The following section focuses on the published power factor graph with individual current harmonics removed. Since the absolute minimum published power factor peaks are unwanted as they reduce the average power factor, they are tabulated in Table 5.3.1 as well as the average published power factor. The power factor graphs with individual current harmonics removed are shown in Fig. 5.3.8.
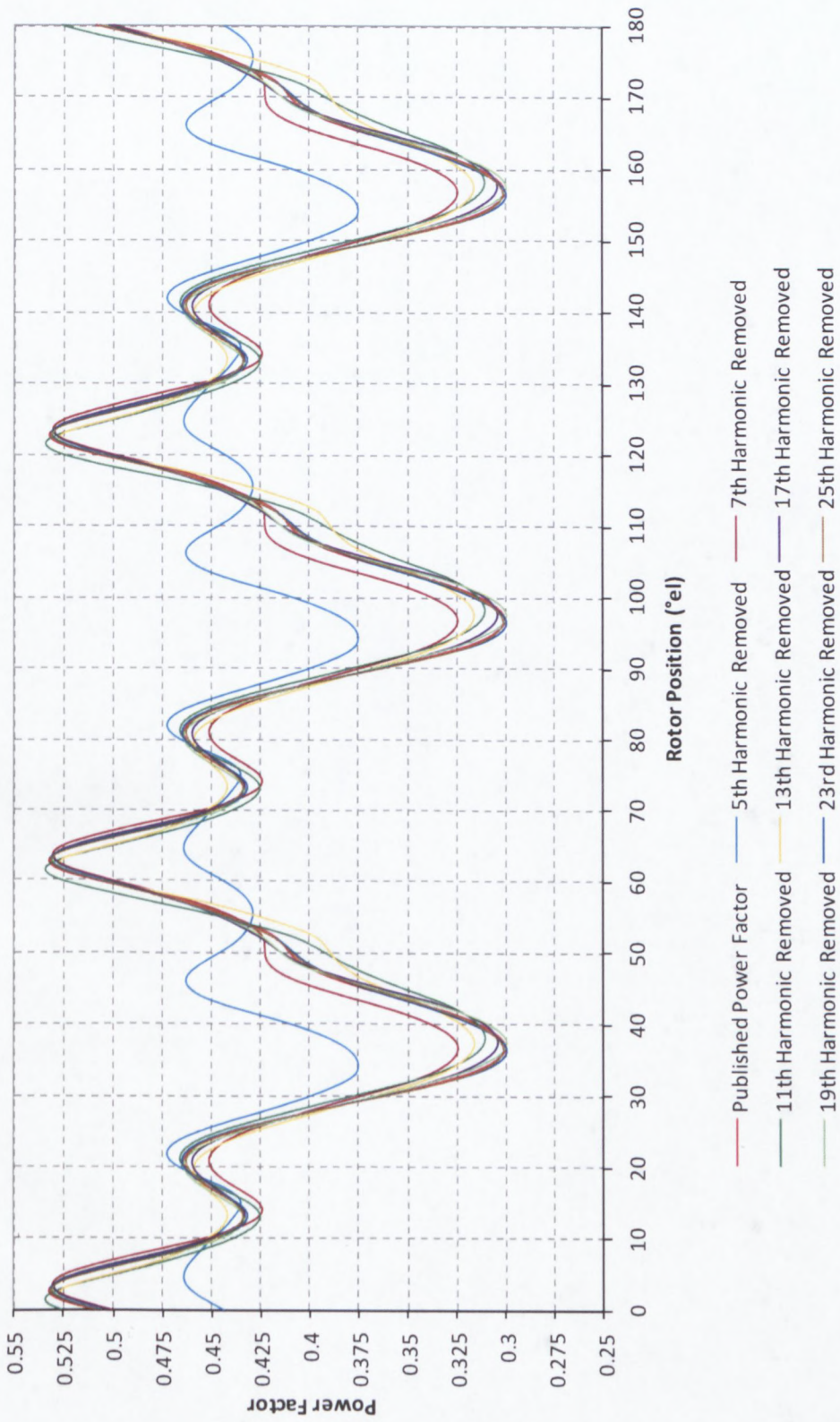
Fig. 5.3.8 Power factor graphs with individual current harmonics removed

Table 5.3.1 Absolute minimum and average published power factor when individual current harmonics is removed

	Absolute Minimum Power Factor	Average Power Factor
Published Power Factor	0.302	0.418
5th Current Harmonic Removed	0.39	0.436
7th Current Harmonic Removed	0.327	0.424
11th Current Harmonic Removed	0.31	0.418
13th Current Harmonic Removed	0.316	0.416
17th Current Harmonic Removed	0.305	0.419
19th Current Harmonic Removed	0.3	0.418
23rd Current Harmonic Removed	0.303	0.418
25th Current Harmonic Removed	0.304	0.418

From Table 5.3.1 it is evident that the 5th current harmonic has the greatest effect on the published power factor. This is clearly visible from Fig. 5.3.8. Without the 5th current harmonic the absolute minimum increases by 29% and the average only by 4.3% which is very little. All other current harmonics have only a slight effect on the published power factor. This is due to the high 5th harmonic current magnitude compared to the rest of the harmonic currents.

The published output power of the machine is shown in Fig. 5.3.9. The ideal and fundamental power is also shown for easy reference.
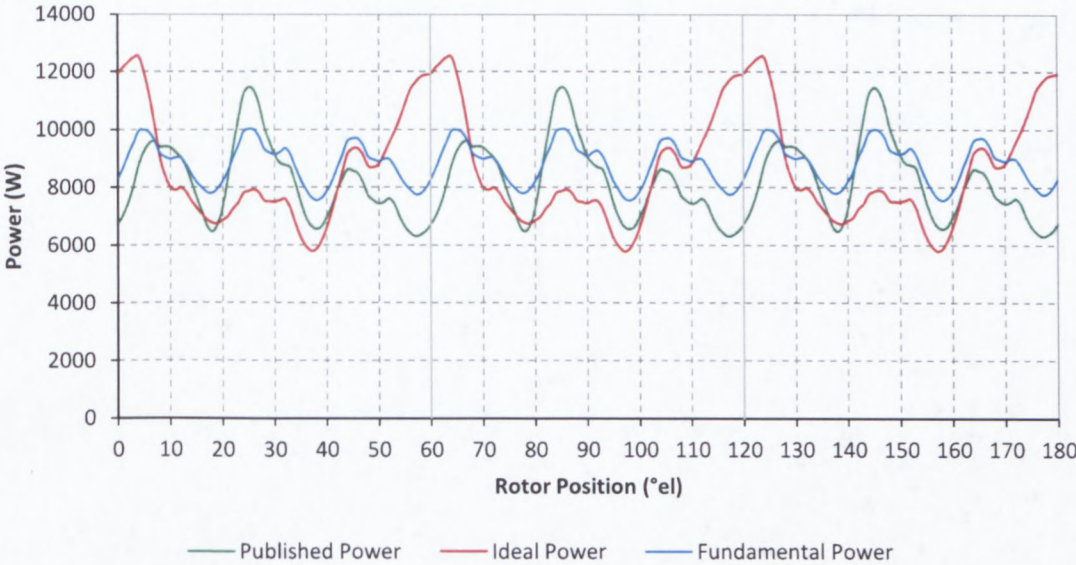
Fig. 5.3.9 Published, ideal and fundamental power as a function of rotor position

From Chapter 4.3 it is known that the angular velocity is constant, therefore the power will show the same dependency on removing current harmonics than the torque. The absolute maximum of the published power is 8.28% lower than the absolute maximum of the ideal power and 15.25% higher than the fundamental power. The published average power however is 5.27% lower than the ideal average power and 7.16% lower than the fundamental power. Therefore the published harmonic currents have a negative effect on the average power while the ideal harmonic currents almost have no effect.

The following table shows the published power graph with individual current harmonics removed. The absolute maximum and average published power are tabulated in Table 5.3.2.

Table 5.3.2 Absolute maximum and average published power when individual current harmonics is removed

	Absolute Maximum Power (W)	Average Power (W)
Published Power	11467.1	8181.98
5th Current Harmonic Removed	9754.7	8710.59
7th Current Harmonic Removed	11851.8	8302.58
11th Current Harmonic Removed	11199.7	8248.42
13th Current Harmonic Removed	11579.4	8191.68
17th Current Harmonic Removed	11363.2	8170.27
19th Current Harmonic Removed	11496.4	8189.04
23rd Current Harmonic Removed	11478.8	8186.59
25th Current Harmonic Removed	11476.3	8185.95

Table 5.3.2 shows that the removal of the 5th current harmonic produces the highest change in published power. The absolute maximum decreases by 14.93% while the average increases by 6.45% to a value of 8710.59 W which is almost equal to the fundamental average power. This shows that all current harmonics except the 5th have minor effects on the average power.

5.4   Winding losses and efficiency

The published winding loss of the RSM is calculated to be 1551.81 W according to equation (2.1.26). This is only 1.91% lower than the ideal winding loss. The published efficiency is shown in Fig. 5.4.1. The ideal and fundamental efficiencies are also shown for easy reference.
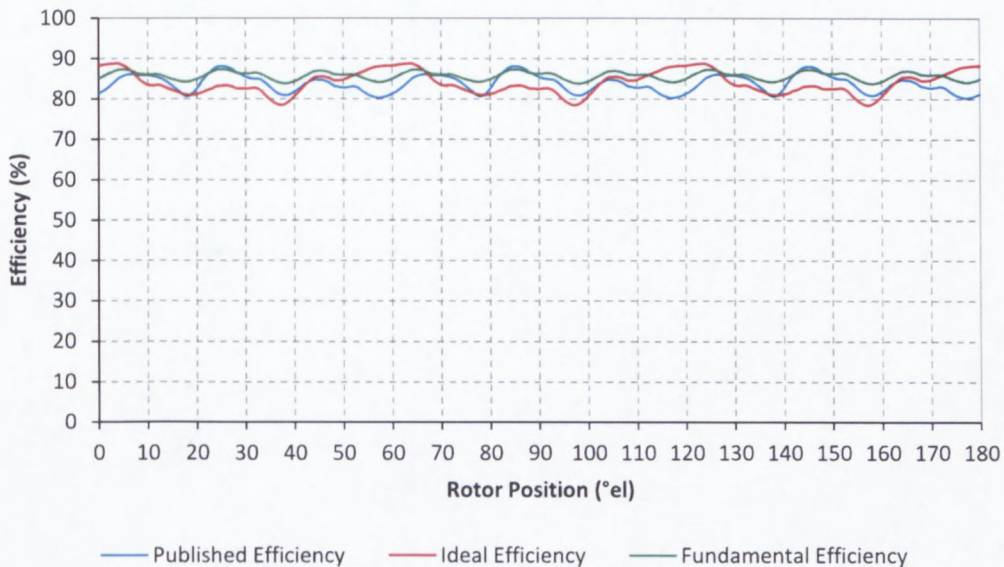
Fig. 5.4.1 Published, ideal and fundamental efficiency as a function of rotor position

The graphs show that the published efficiency does not differ much from the ideal and fundamental efficiency. The average published efficiency is only 0.23% lower than the ideal efficiency and 1.96% lower than the fundamental efficiency. From Chapter 4.4 it is known that the published winding losses are constant. Therefore the published efficiency graph will follow the same pattern than the published power. The average published efficiency graph and winding losses are tabulated in Table 5.4.1 with individual current harmonics removed.

Table 5.4.1 Published efficiency and winding loss with individual current harmonics
removed

	Average Efficiency (%)	Winding Losses (W)
Published Efficiency	83.77	1551.81
5th Current Harmonic Removed	85.42	1471.1
7th Current Harmonic Removed	83.94	1546.41
11th Current Harmonic Removed	83.88	1548.76
13th Current Harmonic Removed	83.82	1549.23
17th Current Harmonic Removed	83.79	1551.34
19th Current Harmonic Removed	83.76	1551.54
23rd Current Harmonic Removed	83.78	1551.73
25th Current Harmonic Removed	83.78	1551.77

From Table 5.4.1 it is evident that without the 5th current harmonic the highest change in winding loss and efficiency is produced. The winding loss reduces by 5.2% causing the published efficiency to gain 1.65%.

5.5 Summary of findings

The findings of chapter 5 are summarized as follows:

- Due to the published harmonic currents not having very high peaks the published torque ripple is 14.93% less than the ideal torque ripple. The average torque decreased by only 5.27%.

- Removing the 5th current harmonic again shows the best result for torque ripple as it reduces the 9th torque harmonic (which is the most dominant) by 27.8% and the 3rd torque harmonic (which is the second most dominant) by 29.6% which results in the torque ripple to decrease by 22.13%. With the absence of the 5th current harmonic the published torque has a slight resemblance to the fundamental torque.

- The published harmonic currents have a slightly negative effect on the average published power factor which is therefore 4.55% lower than the ideal and fundamental average power factors.

- Removing the 5th current harmonic causes the average published power factor to increase and almost equal the ideal and fundamental power factors.

- When published harmonic currents are added the average power is negatively affected but the removal of the 5th published current harmonic causes it to be almost equal to the fundamental average power.

- The published current harmonics have very little effect on the efficiency since the 5th current harmonic reduces the copper loss by only 5.2% (which is the highest individual contribution) and therefore the efficiency increases by 1.65%.

6. Conclusions and Recommendations

In this section all the findings of chapters 4 and 5 will be summarised and recommendations with respect to future research will be given.

6.1 Conclusions

The aim of this thesis was to compare performance parameters of a RSM supplied by purely sinusoidal and non sinusoidal currents. The investigated harmonics were chosen from a standard 6 pulse drive according to equation (4.1). The data for the harmonics to be added are found in two ways namely

1) By pure mathematics i.e. from classic theory.

2) By measurements i.e. from industry.

As a consequence these cases were compared to each other in order to see what the difference between theoretically predicted values (in this thesis called "ideal") and practical values (in this thesis called "published") are. The measurements were taken from industry accepted data given by Anonymous (2000).

Chapter 4 reveals that the torque ripple increases due to the ideal harmonic currents producing very high peaks in the ideal torque. The torque ripple increased by 49.97% compared to the fundamental torque ripple. The average torque however reduced with only 2%. The most dominant ideal torque harmonic was the 3rd while the most dominant fundamental torque harmonic was the 9th. By removing the 5th ideal current harmonic the 3rd ideal torque harmonic reduced by 53.5% which is the main cause for the torque ripple to decrease by 15.97%. The ideal torque ripple is, after the removal of the 5th ideal current harmonic, however still 34.01% higher than the fundamental torque ripple.

The ideal harmonic currents have very little effect on the average power which is also true for the average power factor. The average ideal power is only 2% lower than the average fundamental power and is insignificant compared to the high average value of 8637.52 W. The average power factor of the machine is low with a value of 0.44 due to its low saliency ratio.

The ideal current harmonics had only little effect on the efficiency since the 5th current harmonic reduced the copper loss by only 3.8% (which is the highest individual contribution) and caused the efficiency to increase by only 0.62% to a value of 84.62%. This value is only 1.08% lower than the fundamental efficiency.

Chapter 5 reveals that the published torque ripple is not as high as the ideal torque ripple. This is due to the published harmonic currents not producing very high peaks like the ideal harmonic currents. The published torque ripple increased by 35.04% compared to the fundamental and decreased by 14.93% compared to the ideal torque ripple. The average torque again is however affected slightly. The published average torque is 7.16% lower than the fundamental and 5.27% lower than the ideal average torque. The most dominant published torque harmonic was the 9th which is the same as for the fundamental torque. By removing the 5th published current harmonic the 9th published torque harmonic reduced by 27.8% while the 3rd published torque harmonic, which is the second most dominant harmonic, reduced by 29.6%. This is the main cause for the torque ripple to decrease by a value of 22.13%. The *published* torque ripple is, after the removal of the 5th *published* current harmonic, still 12.92% higher than the *fundamental* torque ripple but 21.45% lower than the *ideal* torque ripple with the 5th *ideal* current harmonic removed. This concludes that ideal harmonic currents cause the torque ripple to increase more than published harmonic currents but the average torque however are similar. It also concludes that there is a difference between the ideal and published harmonic cases. This is further supported by the fact that not all in industry measured harmonic currents are the same.

The published harmonic currents have a slight negative effect on the average power factor but removing the 5th current harmonic causes it to be almost equal to the ideal and fundamental average power factor with a value of 0.44.

The published harmonic currents also have a negative effect on the average published power. The average published power is 5.27% lower than the average ideal power and 7.16% lower than the average fundamental power. Removing the 5th current harmonic causes the published average power to increase by 6.45% to a value of 8710.59 W which is almost equal to the fundamental average power.

The published current harmonics had only little effect on the efficiency since the 5th current harmonic reduces the copper loss only by 5.2% (which is the highest individual contribution) and therefore the efficiency increases by 1.65% to a value of 85.42%. This value is only 0.28% lower than the fundamental efficiency and 0.8% higher than the ideal efficiency with the 5th ideal current harmonic removed.

Overall the results indicate that the 5th current harmonic has the greatest effect on the performance parameters since its magnitude is higher compared to the other harmonics especially in the case of published harmonic currents. It also indicates that the theoretically predicted currents have different effects than the practically measured currents especially in the case of the torque ripple. It has been shown that the ideal case which is mathematically correct does not reflect reality and is worse than the result from measured data. As unsatisfying it may be from the academic point of view it provides however a worst case scenario boundary.

6.2   Recommendations

Kamper (2002) concluded that to obtain low torque ripple and minimal effect on torque rating, full-pitch stator windings should be used. Therefore in this thesis a single layer winding was used since it is full-pitched. This thesis revealed that the 5th current harmonic in both the ideal and published harmonic cases has the highest influence on the performance parameters of all harmonics. The designer should therefore try to eliminate the 5th current harmonic which automatically leads to an investigation into double layer windings because the machine should be build with a certain pitch factor. Since the pitch factor can be non-integer it could also be investigated whether to use the next highest or lowest integer as the pitch factor.

At the end of the last 3 chapters the efficiency was calculated considering only the winding losses. Therefore it is proposed to do this research including the iron losses.

7. References

Anon. 2000. Power Station 3.0, Operation Tecnology Inc., CA, June.

Bianchi, N., Bolognani, S., Bon, D. & Dai Pré, M. 2009. Rotor Flux-Barrier Design for Torque Ripple Reduction in Synchronous Reluctance and PM-Assisted Synchronous Reluctance Motors. *IEEE Trans*, 45(3): 921-928, May/June.

Blondel, A. 1913. Synchronous Motors and Converters. 141-145.

Chang, L., Eastham, A.R. & Dawson, G.E. 1989. Permanent Magnet Synchronous Motor: Finite Element Torque Calculations, *IEEE Industry Applications Society Annual Meeting 24th*, San Diego, USA, :69-73, October.

Cruickshank, A.J.O., Anderson, A.F. & Menzies, R.W. 1971. Theory and performance of reluctance motors with axially laminated anisotropic rotors. *IEE Proc*, 118: 7, July.

Douglas, J.F.H. 1956. The theory of anisotropic field structures in synchronous machines. *AIEE Journal*, 75:84-86.

Eguiluz, L.I. 1999. Performance Analysis of a Three-phase Induction Motor under Non-sinusoidal and Unbalanced Conditions. Department of Electrical Engineering, University of Cantabria, Spain.

Fratta, A., Troglia, G.P., Vagati, A. & Villata, F. 1993. Evaluation of Torque Ripple in High Performance Synchronous Reluctance Machines. *IEEE-IAS 28th Annual Meeting*, 1:163-170, Oct.

Güemes, J.A., Iraolagoitia, A.M., Del Hoyo, J.I. & Fernándes, P. 2011. Torque Analysis in Permanent-Magnet Synchronous Motors: A Comparitive Study, IEEE Transactions on Energy Conversion, 26(1): 55-63, March.

Hanekom, A.N. & Voss, E. 2006. A Torque Ripple Analysis on Reluctance Synchronous Machines. Unpublished Masters Dissertation, Cape Peninsula University of Technology, September.

Hanekom, A.N. 2004. A Study on Torque Harmonics in Reluctance Synchronous Machines. Unpublished Bachelors dissertation, Cape Technikon, December

Hofmann, H. & Sanders, S.R. 2000. High-Speed Synchronous Reluctance Machine with Minimized Rotor Losses. *IEEE Transactions on Industry Applications*, 36(2):531-539, March/April.

Honsinger, V.B. 1971. The inductances L_d and L_q of reluctance machines. *IEEE Trans*, 90:1, January.

Howe, G.W.O., 1935. Some magnetic misconceptions, The Electrician, :601-602, November

Kamper, M.J. 1996. Design Optimization of Cageless Flux Barrier Rotor Reluctance Synchronous Machine. Unpublished PhD dissertation, University of Stellenbosch, December

Kamper, M.J. & Bomela, X.B. 2002. Effect of Stator Chording and Rotor Skewing on Performance of Reluctance Synchronous Machine. *IEEE Trans,* 38(1): 91-100, January/February.

Kamper, M.J. & Fick, P.D. 2002. Accurate Digital Current Control of the Reluctance Synchronous Machine with Constant Current Angle. *IEEE Trans,* 47-50, October.

Kamper, M.J. & Volschenk, A.F. 1994. Effect of rotor dimensions and cross magnetization on Ld and Lq inductances of reluctance synchronous machines with cageless flux barrier rotor. *IEE Proceedings on Electrical Power Applications.*, 141(4):213-220, July.

Kostko, J.K. 1923. Polyphase reaction synchronous motors. *AIEE Journal*, 42:1162-1168.

Lawrenson, P.J. & Gupta, S.K. 1967. Developments in the performance and theory of segmental-rotor reluctance motor. *IEE Proc*, 114(5):645-653, May.

Lee, J.W., Kim, H.S., Kwon, B.I. & Kim, B.T. 2004. New Rotor Shape Design For Minimum Torque Ripple of SRM Using FEM. *IEEE Trans. on Magnetics*, 40(2):754-757, March.

Lin, C.Y. 1951. Characteristics of Reluctance Machines. *AIEE Journal*, 70(2):1971-1977.

Lipo, T.A. & Krause P.C. 1967. Stability Analysis of a Reluctance-Synchronous machine. *IEEE Trans*, 86(7): 825-834, July.

Lipo, T.A. & Matsuo T. 1994. Rotor Design Optimization of Synchronous Reluctance Machine. *IEEE Trans*, 9(2): 359-365, June.

Sanada, M., Hiramoto, K., Morimoto,S. & Takeda, Y. 2004. Torque Ripple Improvement for Synchronous Reluctance Motor Using an Asymmetric Flux Barrier Arrangement. *IEEE Trans,* 40(4): 1076-1082, July/August.

Singh, G.K. 2005. A Research Survey of Induction Motor Operation with Non-sinusoidal Supply Waveforms. Department of electrical engineering, Indian institute of technology, 75: 200-213, May.

Sturgess, J.P. 1987. Finite Element Electromagnetic Analysis of Generator Transient Performance. Unpublished PhD dissertation, University of London, 14, October

Talaat M.E. 1951. Steady-state and transient synthesis of 3-phase reluctance motors. *AIEE Journal*, 70(2):1963-1970.

Thompson, S.P. 1902. Dynamo electric machinery. 8th ed. New York: M Strong: 389.

Trickey, P.H. 1946. Performance calculations on polyphase reluctance motor. *AIEE Journal*, 65:191-193.

Turner, P.J.   1981.   Finite Element Electromagnetic Analysis of Turbine-Generator Performane. Unpublished PhD dissertation, University of London, 2, November.

Vagati, A., Pastorelli, M., Franceschini, G. & Petrache, S.C. 1998. Design of Low-Torque-Ripple Synchronous Reluctance Motor. *Trans IEEE*, 34(4):758-764, July.

Wignall, A.N., Gilbert, A.J. & Yang, S.J. 1988. Calculation of Forces on Magnetised Ferrous Cores using the Maxwell Stress Method, *IEEE Transactions on Magnetics,* 24(1): 459-462, January.

Appendix A

Transformation of currents using Park's Transformation

The transformation is used to transform a set of variables from a stationary system to a rotating system and vice versa. Therefore the stator input currents can be transformed from the stator reference frame to the rotor reference frame and vice versa by applying the following equations

$$i_{dq0} = K \cdot i_{RYB} \tag{A.1}$$

$$i_{RYB} = K^{-1} \cdot i_{dq0} \tag{A.2}$$

where K and K^{-1} are defined as

$$K = \frac{2}{3} \begin{bmatrix} \cos(\omega t) & \cos(\omega t - 120°) & \cos(\omega t + 120°) \\ -\sin(\omega t) & -\sin(\omega t - 120°) & -\sin(\omega t + 120°) \\ 1/2 & 1/2 & 1/2 \end{bmatrix} \tag{A.3}$$

and

$$K^{-1} = \begin{bmatrix} \cos(\omega t) & -\sin(\omega t) & 1 \\ \cos(\omega t - 120°) & -\sin(\omega t - 120°) & 1 \\ \cos(\omega t + 120°) & -\sin(\omega t + 120°) & 1 \end{bmatrix} \tag{A.4}$$

Appendix B

Machine Data

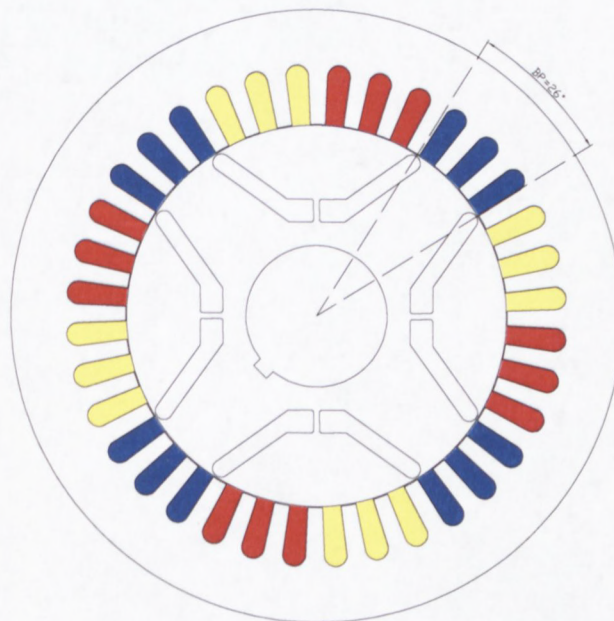|		
Full load voltage	=	443.189 V (rms)
Full load current	=	16 A (rms)
Steady state frequency	=	50 Hz
Number of slots	=	36
Number of slots per ppg	=	3
Core length	=	133.4 mm
Slot pitch	=	10°
Winding layout	=	Single Layer
Pole pitch	=	9 slots
Flux barrier	=	Single
Flux barrier pitch	=	26°

Fig. B.1 Cross section of the RSM

CAPE PENINSULA
UNIVERSITY OF TECHNOLOGY